





Release of ATP by pre-Bötzinger complex astrocytes contributes to the hypoxic ventilatory response via a Ca²⁺-dependent P2Y₁ receptor mechanism

Vishaal Rajani^{1,6} , Yong Zhang¹, Venkatesh Jalubula¹, Vladimir Rancic¹ , Shahriar SheikhBahaei^{2,5}, Jennifer D. Zwicker¹, Silvia Pagliardini¹ , Clayton T. Dickson³, Klaus Ballanyi¹, Sergey Kasparov⁴, Alexander V. Gourine⁵ and Gregory D. Funk¹ 

¹Department of Physiology, Neuroscience and Mental Health Institute (NMHI), Women and Children's Health Research Institute (WCHRI), Faculty of Medicine and Dentistry, University of Alberta, Edmonton, Alberta, Canada

²Cellular and Systems Neurobiology Section, National Institute of Neurological Disorders and Stroke (NINDS), National Institutes of Health (NIH), Bethesda, MD, USA

³Department of Psychology, Neuroscience and Mental Health Institute (NMHI), Faculty of Science, Edmonton, Alberta, Canada

⁴Department of Physiology, Pharmacology and Neuroscience, University of Bristol, Bristol, UK

⁵Centre for Cardiovascular and Metabolic Neuroscience, Neuroscience, Physiology & Pharmacology, University College London, London, UK

⁶Present address: Neurosciences & Mental Health, Peter Gilgan Centre for Research and Learning (PGCRL), The Hospital for Sick Children, Toronto, Ontario, Canada

Key points

- The ventilatory response to reduced oxygen (hypoxia) is biphasic, comprising an initial increase in ventilation followed by a secondary depression.
- Our findings indicate that, during hypoxia, astrocytes in the pre-Bötzinger complex (preBötC), a critical site of inspiratory rhythm generation, release a gliotransmitter that acts via P2Y₁ receptors to stimulate ventilation and reduce the secondary depression.
- *In vitro* analyses reveal that ATP excitation of the preBötC involves P2Y₁ receptor-mediated release of Ca²⁺ from intracellular stores.
- By identifying a role for gliotransmission and the sites, P2 receptor subtype, and signalling mechanisms via which ATP modulates breathing during hypoxia, these data advance our understanding of the mechanisms underlying the hypoxic ventilatory response and highlight the significance of purinergic signalling and gliotransmission in homeostatic control.
- Clinically, these findings are relevant to conditions in which hypoxia and respiratory depression are implicated, including apnoea of prematurity, sleep disordered breathing and congestive heart failure.

Abstract The hypoxic ventilatory response (HVR) is biphasic, consisting of a phase I increase in ventilation followed by a secondary depression (to a steady-state phase II) that can be life-threatening in premature infants who suffer from frequent apnoeas and respiratory depression. ATP released in the ventrolateral medulla oblongata during hypoxia attenuates the secondary depression. We explored a working hypothesis that vesicular release of ATP by astrocytes in the pre-Bötzinger Complex (preBötC) inspiratory rhythm-generating network acts via P2Y₁ receptors to mediate this effect. Blockade of vesicular exocytosis in preBötC astrocytes bilaterally (using an adenoviral vector to specifically express tetanus toxin light chain in astrocytes) reduced the HVR in anaesthetized rats, indicating that exocytotic release of a gliotransmitter within the preBötC contributes to the hypoxia-induced increases in ventilation. Unilateral blockade of P2Y₁ receptors in the preBötC via local antagonist injection enhanced the secondary respiratory depression, suggesting that a significant component of the phase II increase

in ventilation is mediated by ATP acting at P2Y₁ receptors. *In vitro* responses of the preBötC inspiratory network, preBötC inspiratory neurons and cultured preBötC glia to purinergic agents demonstrated that the P2Y₁ receptor-mediated increase in fictive inspiratory frequency involves Ca²⁺ recruitment from intracellular stores leading to increases in intracellular Ca²⁺ ([Ca²⁺]_i) in inspiratory neurons and glia. These data suggest that ATP is released by preBötC astrocytes during hypoxia and acts via P2Y₁ receptors on inspiratory neurons (and/or glia) to evoke Ca²⁺ release from intracellular stores and an increase in ventilation that counteracts the hypoxic respiratory depression.

(Resubmitted 5 June 2017; accepted after revision 27 June 2017; first published online 5 July 2017)

Corresponding author G. D. Funk: 3-020G Katz Group Centre, Department of Physiology, University of Alberta, Edmonton, Alberta, T6G 2E1, Canada. Email: gf@ualberta.ca

Abbreviations aCSF, artificial cerebrospinal fluid; AP5, D-(–)-2-amino-5-phosphonopentanoic acid; AVV, adenoviral vector; BME, Basal Medium Eagle; CNQX, 6-cyano-7-nitroquinoxaline-2,3-dione; CPA, cyclopiiazonic acid; DIA, diaphragm; DLH, DL-homocysteic acid; eGFP, enhanced green fluorescent protein; GFAP, glial fibrillary acidic protein; GG, genioglossus; HVR, hypoxic ventilatory response; IP₃, inositol triphosphate; PLC, phospholipase C; PNA, phrenic nerve amplitude; preBötC, pre-Bötzinger complex; SERCA, sarco/endoplasmic reticulum Ca²⁺-ATPase; TeLC, tetanus light chain; TMPAP, transmembrane prostatic acid phosphatase; \dot{V}_E , minute ventilation; VLM, ventrolateral medulla; VRC, ventral respiratory column; V_T, tidal volume.

Introduction

Acute exposure of mammals to moderate hypoxia evokes a biphasic hypoxic ventilatory response (HVR), comprising an initial increase in ventilation within the first minute followed by a secondary depression to a lower steady-state (Moss, 2000). The initial, phase I increase is primarily attributed to activation of the carotid body chemoreceptors. The secondary depression to a lower steady-state, phase II level is largely central in origin (Teppema & Dahan, 2010). It is also implicated in cardiovascular diseases that accompany obstructive sleep apnoea (Horner, 2012) and may also be a factor in sudden explained death in epilepsy (So, 2008). Interestingly, the HVR changes developmentally. In adults, ventilation during phase II remains above baseline. Newborn mammals experience a similar phase I increase in ventilation, although this is followed by a much larger respiratory depression during which ventilation falls below baseline (Moss, 2000). As a result, infants who suffer from apnoea of prematurity experience frequent apnoeas that can lead to a life-threatening positive feedback loop in which apnoea causes hypoxia leading to respiratory depression and greater hypoxia. Despite its clinical significance, the underlying mechanisms are poorly understood, reflecting, in part, variability in the severity of hypoxic stimulus used to study the HVR, as well as developmental and species differences in the magnitude of the depression and its underlying mechanisms (Funk, 2013).

A role for ATP-mediated purinergic signalling in shaping the HVR is supported by data showing the release of ATP at the ventrolateral medullary surface and an enhanced secondary respiratory depression following

application of P2 receptor antagonists *in vivo* (Gourine *et al.* 2005; Gourine & Funk, 2017). In the *in vitro* rhythmic slice preparation, the activation of P2 (specifically P2Y₁) receptors in the pre-Bötzinger complex (preBötC, a key site of inspiratory rhythm generation) produces a robust two- to four-fold increase in the frequency of fictive inspiratory burst activity (Lorier *et al.* 2007). Additionally, unanaesthetized rats transfected to express transmembrane prostatic acid phosphatase (TMPAP, a potent ectonucleotidase) in the ventrolateral medulla (VLM) to reduce endogenous levels of extracellular ATP, or tetanus toxin light chain (TeLC) protein to block vesicular release specifically in astrocytes, exhibit a decreased HVR (Angelova *et al.* 2015). Astrocytes are the probable source of ATP because they have a mitochondria-based hypoxia sensing mechanism that can evoke vesicular release of ATP (Angelova *et al.* 2015). Exocytotic release of ATP from astrocytes may contribute directly to the homeostatic hypoxic ventilatory response (Angelova *et al.* 2015). The sites and mechanisms by which ATP causes ventilation to increase during hypoxia remain to be determined. Our working model, depicted in Fig. 1, proposes that preBötC astrocytes sense reductions in O₂ and respond by releasing calcium from intracellular stores (i), which evokes exocytotic release of gliotransmitters, including ATP (ii). ATP then activates P2Y₁ receptors located on preBötC inspiratory neurons (iii), which leads to phospholipase C (PLC)-mediated release of calcium from intracellular stores (iv), and the modulation of downstream ion channels via DAG/inositol triphosphate (IP₃) or the activation of protein kinase C (v).

Within this framework, we first examined the role of gliotransmission in the phase I and II components of the

HVR using a viral approach to disrupt vesicular release specifically within astrocytes of the VLM in anaesthetized, vagotomized adult rats. Second, based on data from rhythmically-active brainstem slices demonstrating that ATP excitation of the preBötC is mediated via P2Y₁ receptors (Funk *et al.* 1997; Lorier *et al.* 2004, 2007, 2008; Huxtable *et al.* 2009; Zwicker *et al.* 2011), we tested, in anaesthetized rats *in vivo*, whether ATP released during hypoxia acts in the preBötC via P2Y₁ receptors to increase ventilatory output and attenuate the secondary depression. Finally, P2Y₁ receptors on neurons and astrocytes in other brain regions signal primarily through the G_{αq/11} G-protein coupled receptor pathway to activate PLC and IP₃-mediated Ca²⁺ release from intracellular stores (Simon *et al.* 1995; von Kugelgen & Wetter, 2000; Sak & Illes, 2005), which modulates neuronal excitability or transmitter release through [Ca²⁺]_i-dependent signalling. To assess the role of the G_{αq/11} signalling pathway in mediating the excitatory actions of P2Y₁ receptors on the preBötC network, we used rhythmic medullary slices from neonatal rats to compare the effects of P2Y₁ receptor activation on: (i) the network response before and after chelating intracellular calcium and inhibiting sarco/endoplasmic reticulum Ca²⁺ ATPase (SERCA) and (ii) the calcium response evoked in inspiratory neurons and preBötC glia by P2Y₁ receptor activation before and after SERCA inhibition. These data advance our understanding of the sites, receptor mechanisms and signalling cascades that underlie the contribution of astroglial purinergic signalling to the HVR.

Methods

All the experiments were performed in accordance with the guidelines of the Canadian Council on Animal Care and European Commission Directive 2010/63/EU (European Convention for the Protection of Vertebrate Animals used for Experimental and Other Scientific Purposes) with project approval from the respective Institutional Animal Care and Use Ethics Committees.

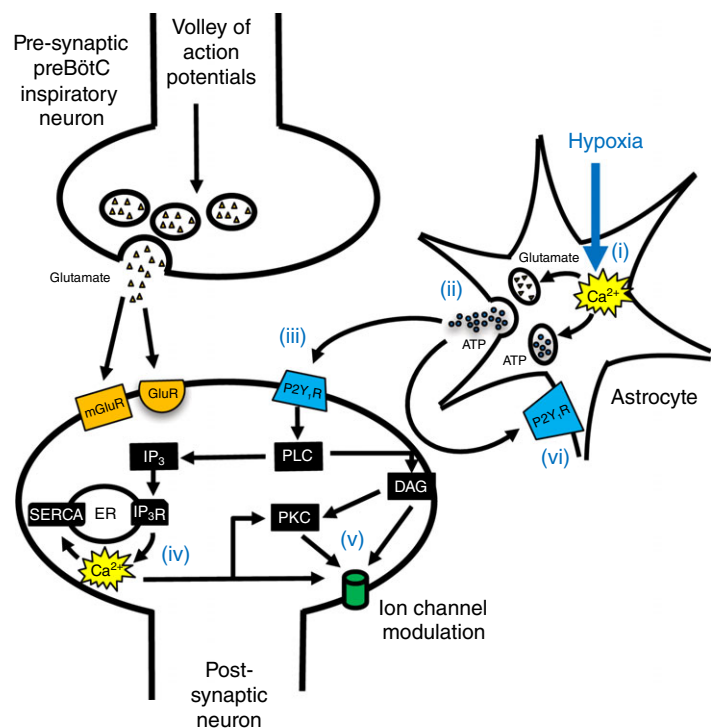
In vivo methods

Adult *in vivo* preparations. Adult male Sprague–Dawley rats (250–350 g) were anaesthetized using isoflurane (3% in 100% O₂) and the femoral vein was cannulated. Isoflurane anaesthesia was then replaced with urethane (1.5–1.7 g kg⁻¹) delivered intravenously (i.v.). Additional doses of urethane were given as necessary. The femoral artery was cannulated to monitor arterial blood pressure and blood gases in some experiments (as described below). The trachea was cannulated, and the vagus nerves resected bilaterally at the mid-cervical level to eliminate confounding effects of vagal reflex stimulation. Vagotomy produced a well-described reduction in respiratory frequency. Baseline respiratory frequency was within a range of 40–55 breaths min⁻¹ in anaesthetized, mechanically ventilated, spontaneously breathing rats. From this point, there were two variations of the preparation.

For hypoxia experiments, rats were paralysed with gallamine triethiodide or pancuronium bromide

Figure 1. Purinergic modulation of respiratory rhythm: a working hypothesis

At the synapse of two preBötC inspiratory neurons, volleys of action potentials during inspiration in the presynaptic neuron evoke glutamate release, exciting postsynaptic neurons via ionotropic (GluR) and metabotropic (mGluR) receptors on preBötC inspiratory neurons. During hypoxia, astrocytes sense changes in O₂, causing increases in intracellular calcium (i), resulting in the exocytotic release of gliotransmitters, including ATP (ii). ATP acts via P2Y₁ receptors located on preBötC neurons (iii), causing a release of Ca²⁺ from intracellular stores mediated by DAG/IP₃ (iv), and the modulation of downstream ion channels, [Ca²⁺]_i, or the activation of protein kinase C (PKC) (v). Autocrine/paracrine of astrocytes by ATP may also contribute (vi).



(10 mg kg⁻¹ i.v.; 1 mg kg⁻¹) and mechanically ventilated with a mix of 20% or 30% O₂, balance N₂ (1 l min⁻¹, 60 strokes min⁻¹ at ~2 ml stroke⁻¹, for a tidal volume of 8 ml kg⁻¹). Paralysis and mechanical ventilation were used to open chemoreflex loops so that changes in central respiratory drive would not affect blood gases. Expired CO₂ was monitored continuously from a small port in the tracheal tube (PowerLab gas analyser, ML206; AD Instruments, Colorado Springs, CO, USA) and remained constant during the experimental protocols. However, obtaining a true reading of end-tidal CO₂ (i.e. one that equals PaCO₂) is a challenge in small rodents. Therefore, we measured and report baseline blood gases in the three groups (naïve control, viral control and TeLC expressing rats; as described in more detail below) of experimental animals in the first series of studies that involved viral injections and survival surgeries. Also in the initial hypoxia experiments involving the naïve and viral control groups, we measured blood gases before and during the hypoxic challenge to: (i) ensure that we had control over blood gases; (ii) determine the PaO₂ achieved through pump ventilation with 10% O₂; and (iii) ensure that blood gas and pH values were within physiological ranges and consistent between naïve rats and animals who had undergone survival surgery for viral injection. Because blood gases were consistent between groups (see Results), as expected for paralysed animals on mechanical ventilation, blood gases were not taken during hypoxia in the remaining *in vivo* hypoxia studies (i.e. for the TeLC animals during hypoxia and in subsequent acute experiments involving injection of MRS 2279).

Once the rat was placed in prone position in a stereotaxic device (Kopf Instruments, Tujunga, CA, USA) and mechanically ventilated, the brachial plexus was exposed dorsolaterally behind the right shoulder blade. The phrenic nerve was isolated, cut distally, placed over dual platinum electrodes and embedded in kwik-sil adhesive (World Precision Instruments, Sarasota, FL, USA) for long-term stability and to prevent nerve desiccation.

Experiments that tested the acute effects of locally applying purinergic agonists into the preBötC were conducted in spontaneously breathing animals. The effects on blood gases of agonist-evoked [DL-homocysteic acid (DLH), MRS 2365, adenosine] ventilatory responses were not measured in spontaneously breathing animals because of the short duration of the agonist-evoked responses. Electrodes made from Teflon-coated wires (AM Systems, Carlsborg, WA, USA) were placed in the genioglossus and diaphragm muscles to record electromyographic activity (GG_{EMG} and DIA_{EMG}, respectively). The animal was then positioned in a stereotaxic frame in prone position. Body temperature was maintained at 37°C in all *in vivo* experiments with a servo-controlled heating pad (Harvard Apparatus, Holliston, MA, USA).

Viral gene transfer *in vivo*. Adult male rats (200–250 g) were anaesthetized with a mixture of ketamine (90 mg kg⁻¹ i.p.) and xylazine (10 mg kg⁻¹, i.p.). They were then placed in a stereotaxic frame, where a small craniotomy was performed to expose the obex. Using the co-ordinates described below, adenoviral vectors were injected bilaterally into the preBötC. Glial expression of TeLC and enhanced green fluorescent protein (eGFP) was achieved using a bicistronic adenoviral vector (AVV) construct as previously described, where eGFP expression was linked to TeLC via a ‘SKIP’ sequence (Angelova *et al.* 2015). The bicistronic construct, making use of the viral ribosomal skipping mechanism, allows for a high expression of eGFP at the same time as attenuating TeLC expression to avoid cell toxicity. Vectors contained enhanced shortened glial fibrillary acidic protein (GFAP) promoter to drive the expression of TeLC and eGFP (AVV-sGFAP-eGFP-TeLC). As a control, we used an AVV expressing eGFP only (AVV-sGFAP-eGFP).

Viruses were diluted in HEPES buffer and slowly injected into the preBötC under direct visualization (500 nl over 2 min). Following injection, the pipette remained in place for 5 min before withdrawal. The skin was sutured and the animal was put in postoperative care and closely observed throughout recovery from anaesthesia. Rats were left to recover for 6–8 days before the *in vivo* experiments to ensure stable viral expression. Virus dilution and the post-injection incubation period were established through experiments that involved a series of 10-fold dilutions and incubation periods that varied from 5 to 9 days. Rats were killed at the end of the respective incubation period, perfused and tissue examined to define the dilution and incubation period that provided the strongest glial expression with no evidence of tissue damage. High virus concentrations produced bright yet grainy fluorescence expression and transfected cell bodies near the injection site were hard to locate, consistent with cell death/damage. Low virus concentrations yielded weaker eGFP fluorescence, although individual cell bodies and processes were clearly identifiable. Original viruses of titres 1.4×10^{11} (control) and 2.10×10^{10} (TeLC) were diluted 1:100.

Recording of muscle and nerve activities *in vivo*. *In vivo* recordings of EMG and phrenic nerve activities were amplified using a differential AC amplifier (model 1700; AM-systems, Sequim, WA, USA) and sampled at 2 kHz using a PowerLab 16/30 data acquisition system (AD Instruments, Colorado Springs, CO, USA). Phrenic nerve activity was rectified, bandpass filtered (300 Hz to 1 kHz) and the raw signal was integrated (time constant = 0.08 s) to calculate respiratory frequency and phrenic nerve inspiratory burst amplitude as an index of central respiratory drive.

In vitro slice and glial culture methods

Rhythmically-active medullary slice preparation.

Rhythmically-active medullary slices were obtained from neonatal rats (P0–P4) as described in detail previously (Smith *et al.* 1991; Ruangkittisakul *et al.* 2006; Zwicker *et al.* 2011). Briefly, rats were anaesthetized through inhalation of isoflurane and decerebrated. The brainstem-spinal cord was then isolated in cold artificial cerebrospinal fluid (aCSF) containing (in mM): 120 NaCl, 3 KCl, 1.0 CaCl₂, 2.0 MgSO₄, 26 NaHCO₃, 1.25 NaH₂PO₄, 20 D-glucose and bubbled with 95% O₂–5% CO₂. The brainstem-spinal cord was pinned to a wax chuck, and serial 100–200 μ m sections were cut in the rostral to caudal direction using a vibrating microtome (VT1000S; Leica, Nussloch, Germany). Sections were trans-illuminated to identify anatomical landmarks. The structure of the subnuclei of the inferior olive was particularly useful in defining this boundary. A 700 μ m rhythmic transverse slice containing the preBötC was obtained. Special care was made to ensure that the preBötC was at the rostral surface of the slice (~0.35 mm caudal to the caudal aspect of the facial nucleus) (Smith *et al.* 1991; Ruangkittisakul *et al.* 2006, 2008; Lorier *et al.* 2007). Rhythmic slices were pinned rostral surface up on Sylgard resin in a 5 ml recording chamber and perfused with aCSF at a flow rate of 15 ml min⁻¹ (dead space of perfusion system including inflow and outflow lines and chamber was ~20 ml). The concentration of K⁺ in the aCSF ([K⁺]_e) was raised from 3 to 9 mM at least 30 min before the start of data collection to produce prolonged stable rhythm (Ruangkittisakul *et al.* 2006). Rhythmic slice experiments were conducted at room temperature (24°C).

Primary cultures of glia isolated from the preBötC.

Culture preparation. Cultures were prepared from 300 μ m thick preBötC slices from neonatal rats (P0–P4) as described in detail previously (Huxtable *et al.* 2010). Culture media were used at 37°C. The preBötC region was collected bilaterally using 21 gauge tissue punches. Tissue punches were transferred to separate 15 ml conical tubes, washed (twice) with Dulbecco's PBS (2 ml) (Invitrogen, Carlsbad, CA, USA) and centrifuged (1500 g for 1 min). PreBötC tissue was plated directly on Thermanox plastic coverslips (Invitrogen) and placed in a T25 flask containing Basal Medium Eagle (BME)-glucose (1 ml) that was produced by adding to 1 \times BME solution (Invitrogen): 3.3 mM glucose (final concentration of 8.8 mM), 2 mM L-glutamine (Sigma-Aldrich, St Louis, MO, USA), penicillin/streptomycin (10 000 U of penicillin/10 000 μ g of streptomycin per ml) (Invitrogen) and 10% rat serum.

PreBötC-containing coverslips were incubated in 1 ml of BME-glucose for the first 24 h and 1 ml of BME-sorbitol

(10% rat serum) thereafter. BME-sorbitol was equivalent to BME-glucose, except that D-glucose was replaced with sorbitol (2.5 mM) (Fisher Scientific, Waltham, MA, USA) to select for glia. After 48 h, fresh media (with 2.5% rat serum) was added and changed every 3 days. Cultures were grown for 6 days, smeared, maintained in a 24-well plate for 2 weeks and then imaged.

Recording of nerve and neuronal activities in vitro.

In vitro recordings of inspiratory activity were made using glass suction electrodes (AM Systems, Carlsborg, WA, USA) placed on the XII (hypoglossal) nerve rootlets. Inspiratory-related field potentials were also recorded from the surface of the slice using a four-axis manual manipulator to place a suction electrode (inside diameter 120 μ m) on the surface of the slice over the rostrally-exposed preBötC (Ramirez *et al.* 1996). The pipette was systematically moved in 60 μ m steps until the most robust signal was detected. This technique was used to establish the approximate location of the preBötC to assist local drug injection. Signals were amplified, bandpass filtered (300 Hz to 1 kHz), rectified, integrated and displayed using Axoscope, version 9.2 (Molecular Devices, Sunnyvale CA, USA). Data were saved using a Digidata 1322 A/D board and Axoscope 9.2 software (Molecular Devices) for offline analysis.

Responses of cultured glia were measured using Fluo-4 Ca²⁺ imaging. Cultures were loaded for 45 min (35°C) with the membrane-permeant Ca²⁺-sensitive dye, fluo-4-AM (0.01 mM; Sigma-Aldrich, Oakville, ON, Canada) in aCSF, containing (in mM): 117 NaCl, 5 KCl, 1 NaH₂PO₄, 2 CaCl₂, 1 MgSO₄, 26 NaHCO₃ and 6 glucose. Coverslips were then moved to the recording chamber (3 ml volume, 28°C, 6 ml min⁻¹ flow rate) containing aCSF saturated with 20% O₂, 5% CO₂ and 75% N₂. Fluorescence intensity was measured using an upright microscope (Axioskop2 FS Plus; Zeiss, Oberkochen, Germany) fitted with a 40 \times water-immersion objective (NA = 0.8), xenon arc lamp (175 W; Sutter Instruments, Novato, CA, USA) and a Sensi-Cam QE (PCO Tech, Romulus, MI, USA). Imaging Workbench, version 6.0 (INDEC Bio-Systems, Santa Clara, CA, USA) was used to control a Lambda 10-2 shutter system (Sutter Instruments). Images were acquired at 1 Hz (20 ms exposure). Drugs (ATP 10 μ M and thapsigargin 50 nM) were applied from triple-barrelled micropipettes using a controlled pressure source. Consecutive agonist applications were 10 min apart. The locally-applied ATP concentration was 10-fold lower in these experiments compared to slice experiments because of improved drug access to glial monolayers.

PreBötC inspiratory neuron activity was monitored in rhythmic slices using Fluo-4 Ca²⁺ imaging or whole-cell

recording. In calibrated slices (Ruangkittisakul *et al.* 2006, 2008), the free cytosolic Ca^{2+} concentration ($[\text{Ca}^{2+}]_i$) was monitored by FV1000 MPE multiphoton scanning microscopy (Olympus, Tokyo, Japan). A MaiTai-BB Ti:sapphire femtosecond pulsed laser set to excite at 810 nm was used for fluorescence excitation and an Olympus 20 \times immersion objective (NA = 1.0) was used to image the neurons. The membrane-permeant Ca^{2+} dye fluo-4-AM was pressure-injected (25–50 mmHg, 10 min) into the preBötC using a broken patch pipette filled with aCSF containing 0.5 mM Fluo-4-AM dissolved in dimethyl sulfoxide containing 20% pluronic acid (Sigma-Aldrich, Oakville, ON, Canada). Neurons and glia, stained in an area of 150–300 μm diameter, were imaged at 30–75 μm depths for several hours at scanning rates of 2.5 Hz that are sufficient to resolve peaks of inspiratory-related $[\text{Ca}^{2+}]_i$ rises (Ruangkittisakul *et al.* 2006, 2012).

Whole cell recordings were obtained from preBötC inspiratory neurons in rhythmic slices under direct infrared differential interference contrast microscopy visualization. A horizontal puller (P-97; Sutter Instruments) was used to pull patch pipettes from 1.2 mm (outer diameter) filamented borosilicate glass (Harvard Apparatus, Holliston, MA, USA). Pipette resistance was $5.1 \pm 0.1 \text{ M}\Omega$. The intracellular solution used in the present study contained (in mM): 140 potassium gluconate, 5 NaCl, 1 MgCl_2 , 0.1 EGTA, 10 HEPES and 1 glucose, pH adjusted to 7.25–7.35. Intracellular signals were amplified and filtered (1.8 kHz low-pass Bessel filter) with a MultiClamp 700A amplifier (Molecular Devices), acquired at 1 and 5 kHz using a Digidata 1322A A/D board (Molecular Devices), for Axoscope, version 9.2, and Clampex, version 9.2 (Molecular Devices), respectively, and stored on a computer hard disk for off-line analysis using Clampfit, version 9.2 (Molecular Devices).

ATP was excluded from the intracellular solution because its inclusion would result in P2 receptor desensitization as the solution is pressure ejected from the pipette when approaching the neurons. Recordings were obtained under voltage clamp conditions at a holding potential of -60 mV . Inspiratory neurons were identified based on the presence of rhythmic inward synaptic current inputs that were synchronized with inspiratory-related bursts recorded from the XII nerve rootlets. Neurons without rhythmic inputs were immediately discarded. Recorded neurons had an average resting potential of $-48 \pm 1.3 \text{ mV}$, input resistance values of $189 \pm 40 \text{ M}\Omega$ and series resistance averaged $19.1 \pm 1.5 \text{ M}\Omega$. Short voltage pulses (100 Hz, -10 mV , 3.0 ms) were used to estimate series resistance and whole-cell capacitance. The experiments where series resistance increased over 20% between control and trial conditions were excluded. Input resistance was calculated from the inverse of the slope of a linear regression line fitted to the $I-V$

curves generated by depolarizing ramps from -90 to -40 mV .

Immunohistochemistry

At the end of the experiments, the rats were perfused transcardially with 10% saline (100 ml), followed by 4% paraformaldehyde (100 ml). The brainstem was removed and submersion fixed for at least 24 h in 4% paraformaldehyde solution. The brainstems were sectioned serially into 50 μm slices in PBS solution using a vibratome (VT 1000S; Leica). The preBötC was identified based on anatomical landmarks: $\sim 800 \mu\text{m}$ caudal to caudal border of the facial nucleus, at the same level as the lateral loop of the principal subnucleus of the inferior olive and the semi-compact nucleus ambiguus, just caudal to compact nucleus ambiguus (Paxinos & Watson, 2007; Ruangkittisakul *et al.* 2008). The well-established preBötC marker, NK1 receptor immunolabelling, was also used to define the preBötC. Serial sections were examined for the region of most intense labelling indicative of the preBötC (Guyenet & Wang, 2001; Guyenet *et al.* 2002). MRS 2279 (P2Y₁ receptor antagonist) injection sites were identified via fluorescent microspheres (dilution 1:200; 0.1 μm , yellow–green, 2% solids; Life Technologies, Grand Island, NY, USA). NK1 receptor immunolabelling was examined using a rabbit anti-NK1 receptor primary antibody (dilution 1:1000, catalogue number AB-5060; Millipore, Billerica, MA, USA) with a Cy3-conjugated donkey anti-rabbit secondary (dilution 1:200, catalogue number 711-165-152; Jackson ImmunoResearch, West Grove, PA, USA). To assess viral expression, eGFP fluorescence was enhanced with a chicken anti-GFP primary antibody (1:1000, catalogue number GFP-1020; Aves Labs, Tigard, OR, USA) and an AlexaFluor 488 anti-chicken secondary antibody (catalogue number A-11039; Life Technologies). To check glial specificity of viral expression, we used Cy3-conjugated NeuN rabbit antibody (dilution 1:200, catalogue number ABN78C3; Millipore) to stain neuronal nuclei. Slices were mounted on slides and observed with a fluorescence microscope (DM5500; Leica) and a digital camera (Hamamatsu Photonics, Hamamatsu, Japan). Low magnification images to assess injection site were acquired through MetaMorph (Molecular Devices) acquisition software, and the extent of viral expression analysed using ImageJ (NIH, Bethesda, MD, USA) and Photoshop (Adobe Systems, San Jose, CA, USA). High magnification images were taken with a confocal microscope (TCS SP5; Leica) to assess cellular expression patterns. Brightness and contrast for images were adjusted in ImageJ. All images in a series were adjusted identically. Regions of interest were delineated by identifying NeuN labelled neuronal cell bodies under Cy3 fluorescence and then switching to GFP fluorescence to check for eGFP fluorescence indicative of neuronal expression of virally-transfected protein.

Drugs and their application

In vivo. DLH (1–10 mM) and gallamine triethiodide were obtained from Sigma-Aldrich (St Louis, MO, USA), whereas MRS 2365 (1 mM), adenosine (500 μ M) and MRS 2279 (500 μ M) were obtained from Tocris Biosciences (Bristol, UK). Pancuronium bromide was obtained from Alomone Labs (Jerusalem, Israel). Drugs were made up in HEPES-buffer containing (in mM): 137 NaCl, 5.4 KCl, 0.25 Na₂HPO₄, 0.44 KH₂PO₄, 1.3 CaCl₂·2H₂O, 1.0 MgSO₄·7H₂O, 4.2 NaHCO₃ and 10 Hepes) to maintain neutral pH.

For preBötzing drug injections, the head was tilted in the stereotaxic frame such that bregma was 5 mm below lambda (Gray *et al.* 2001). Drugs or vehicle (HEPES-buffer) were pressure injected (Picospritzer III, Parker, Pine Brook, NJ) into the preBötC through a reticulated, sharp glass pipette (40 μ m tip). The preBötC was located using stereotaxic co-ordinates (in mm) that, relative to obex, were 0.9 rostral, 2.0 lateral and 2.8 ventral. Injection volume was monitored by observing the movement of the meniscus relative to the reticulate. An excitatory response to DLH (1–10 mM) confirmed the location of the preBötC (Monnier *et al.* 2003). With this approach, we were successful in targeting the preBötC on the first pipette tract in 83% of the experiments. In the remaining 17% of experiments, the pipette was moved rostrally or caudally and the expected response was evoked on the second injection. We did not notice any changes in network activity with second insertion of the electrode into the preBötC, although this was not analysed in detail. MRS 2279 solution contained fluorescent microspheres (0.1 μ m, yellow–green, 2% solids; Life Technologies) for histological identification of injection sites in relation to NK1 receptor immunolabelling.

In vitro. ATP (10 μ M), MRS 2365 (10 μ M, 100 μ M), MRS 2279 (500 μ M), DL-2-amino-5-phosphono-pentanoic acid (AP5) (100 μ M), thapsigargin (100 μ M, 200 μ M), cyclopiazonic acid (CPA) (100 μ M) and [Sar⁹-Met(O₂)¹¹]-substance P (1 μ M) were obtained from Tocris Biosciences. 6-Cyano-7-nitroquinoxaline-2,3-dione (CNQX) (10 μ M) and (+)-MK-801hydrogen maleate (MK-801, 100 μ M) were obtained from Sigma-Aldrich (St Louis, MO, USA). TTX (0.5 μ M) was purchased from Alomone Labs. Drugs were prepared as stock solutions in aCSF and frozen in aliquots, except PPADS, suramin, TTX, CNQX, AP5 and MK-801, which were prepared in MilliQ (EMD Millipore, Billerica, MA, USA) water. Thapsigargin and CPA required DMSO (0.2%) for complete solubility. For drugs added *in vitro*, the final concentration of K⁺ in the drug solution was matched to that of the aCSF.

Drugs were injected unilaterally into the preBötC via triple-barrelled pipettes (5–6 μ m per barrel outer

diameter). Drug microinjections were controlled by a programmable stimulator (Master-8; AMPI, Jerusalem, Israel) connected to a picospritzer (~18 psi Spritzer4 Pressure Micro-Injector; Bioscience Tools, San Diego, CA, USA). Consecutive agonist (MRS 2365) applications were separated by a minimum of 15 min. The suction electrode on the surface of the slice was used to guide the initial placement of the pipette. Substance P (1 μ M) was then locally applied to functionally identify the preBötC based on a characteristic immediate, three- to four-fold increase in inspiratory frequency (Lorier *et al.* 2007; Zwicker *et al.* 2011). The injection site was moved in a grid-like fashion until the characteristic response was observed. When drugs (TTX, CNQX, AP5) were added directly to the circulating aCSF, they were given at least 10 min to equilibrate. During fluorescence imaging of inspiratory neurons, thapsigargin/CPA was given 30 min to equilibrate with the slice in a re-circulated bath (5 ml min⁻¹, bath volume; 20 ml).

Statistical analysis

Airflow and electromyographic activity from the genioglossus and diaphragm muscles (GG_{EMG} and DIA_{EMG}) were acquired from spontaneously breathing rats. Airflow was measured via a pneumotach (GM Instruments, Killwinning, UK) connected to a pressure transducer (Validyne, Northridge, CA, USA) attached to the tracheal cannula and this signal was used to obtain frequency, tidal volume (V_T) and minute ventilation (\dot{V}_E). V_T was obtained by integration of the airflow recording and converted to millilitres of air using a five-point calibration curve (range 0.5–5 ml) (Boutin *et al.* 2017). Parameters during drug application were compared with the average value during a 2 min control period preceding drug application. Peak drug effect was defined as the maximum value measured in a moving average of three consecutive bursts during the initial minute after the injection.

Phrenic nerve activity (\int PN), blood pressure and arterial blood gases were measured in paralysed rats. Frequency, integrated phrenic nerve amplitude (\int PNA) and ventilatory output (frequency \times \int PNA) were calculated from the phrenic nerve recording in LabChart (AD Instruments, Sydney, Australia) and then exported to Excel (Microsoft Corp, Redmond, WA, USA) for analysis. Respiratory parameters were calculated from 30 s time bins and reported relative to a 2 min control period preceding drug application. The HVR was characterized by comparing the peak values obtained during the initial hypoxia-induced increase in ventilation (phase I) and during the secondary depression when ventilation had plateaued (phase II). The peak value during phase I represents the group average of individual peak values obtained from a moving average measured during the

first 1.5 min of hypoxia. Phase II values represent the average measured over the last 2 min of hypoxic exposure. All signals from the *in vivo* experiments were acquired and integrated in LabChart (AD Instruments, Sydney, Australia).

XII nerve activity from rhythmic slices was analysed offline using Clampfit, version 9.2 and Excel. To assess the effects of a specific agent on the frequency response evoked by local injection of P2 receptor agonists into the preBötC, we compared the relative increase in peak frequency evoked by the agonist in the control and in the presence of drug. Baseline frequency was the average frequency measured over the 2 min immediately prior to drug application. Peak frequency was the peak value in the first min of drug application obtained from a moving average calculated based on three consecutive XII bursts (Huxtable *et al.* 2010; Zwicker *et al.* 2011).

Differences between means were compared using either Prism, version 4 (GraphPad Software Inc., La Jolla, CA, USA) or SPSS, version 20 (IBM Corp., Armonk, NY, USA). For comparison of two groups, paired or unpaired *t* tests were used as appropriate. For comparison of more than two groups, ANOVA was used in conjunction with either a Tukey or Bonferroni *post hoc* multiple comparison test. Unless specified otherwise, *n* refers to the number of rats. $P < 0.05$ was considered statistically significant. Group data are presented as box plots created by the web-application 'BoxPlotR' (Spitzer *et al.* 2014). Each box plot details the spread of data points, which are superimposed on each box. Whiskers are defined by the lowest point, first quartile, median, third quartile and highest point, denoted by the lower whisker, bottom, middle, top of box and top whisker, respectively. The mean for each group is denoted by a plus symbol (+).

Results

Astroglial vesicular mechanisms contribute to the hypoxic ventilatory response *in vivo*

The overall reduction in the ventilatory response of conscious adult rats to hypoxia in conditions of TeLC expression in astrocytes of the ventrolateral medulla, including the preBötC (Angelova *et al.* 2015), indicates a significant contribution of medullary astroglia to the hypoxia-induced increase in ventilation, by the release of gliotransmitters, as shown in Fig. 1(ii). The HVR, however, is biphasic. Thus, our first objective was to re-examine the contribution of glial vesicular release mechanisms by focusing on phases I and II of the HVR,

5 to 7 days after viral injection, the rats were anaesthetized, paralysed, vagotomized and mechanically ventilated. Phrenic nerve activity, blood pressure and blood gases were monitored and the HVR was compared between three groups of rats: naïve, control rats expressing

eGFP in preBötC astrocytes *vs.* rats expressing TeLC and eGFP in preBötC astrocytes. Baseline parameters were measured in normoxia (30% O₂/70% N₂) for 2 min. Baseline respiratory frequency, partial pressures of arterial PO₂ and PCO₂, and arterial pH were similar in control, viral control and TeLC expressing groups (Fig. 2). Mean arterial pressures were also similar in naïve control rats (112.06 ± 4.92 mmHg) and TeLC-expressing rats (97.91 ± 12.69 mmHg), although they were elevated in the viral control group (137.15 ± 4.52 mmHg, one-way ANOVA, Tukey's *post hoc* test, $P = 0.008$). Rats were then exposed to 5.5 min of hypoxia (10% O₂, 90% N₂) and returned to normoxia for 2 min. Sample traces from individual control and TeLC rats, as well as time courses calculated for group data, are shown in Fig. 3A and B and reported relative to baseline. Comparisons of phase I and II parameters for the three groups are reported in Fig. 3C. During phase I, the frequency and amplitude of the phrenic nerve discharge in naïve rats ($n = 10$) increased to a maximum of 1.41 ± 0.10 and 1.30 ± 0.04 of baseline, respectively, giving a ventilatory output that was 1.79 ± 0.13-fold greater than the baseline. Rats transduced to express eGFP ($n = 6$) showed similar phase I increases in frequency, amplitude and the overall

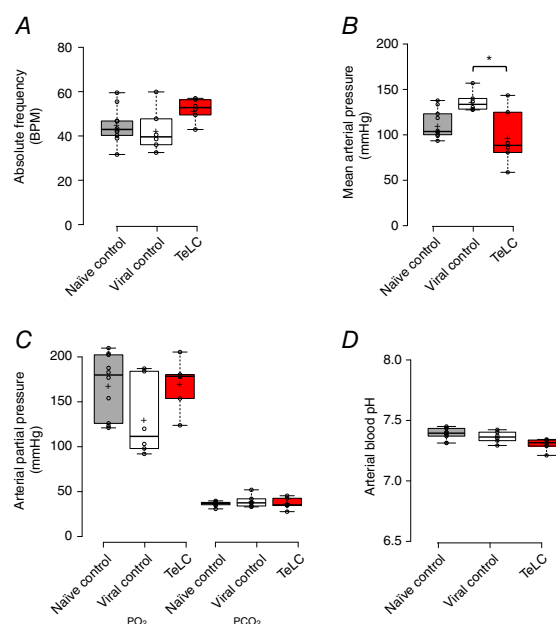


Figure 2. Baseline parameters in the naïve control rats and rats transduced to express eGFP or TeLC in the preBötC astrocytes

Group data indicating the absolute values of respiratory frequency (A), mean arterial pressure (B), arterial PO₂ and PCO₂ (C), and pH (D) under baseline conditions, prior to the administration of hypoxia for the naïve control and viral control, as well as the TeLC expressing rats. An asterisk (*) indicates significant difference between means ($P < 0.05$, one-way ANOVA, Tukey's *post hoc* test).

ventilatory output of 1.35 ± 0.04 , 1.44 ± 0.09 and 1.83 ± 0.09 , respectively. The phase I response of rats expressing TeLC in medullary astrocytes was significantly reduced. Frequency and \int PNA were 1.16 ± 0.03 ($n = 6$) and 1.25 ± 0.04 ($n = 6$) of the control. Ventilatory output increased to 1.35 ± 0.06 ($n = 6$) of baseline, which was significantly smaller than in the naïve rats and rats transduced to express eGFP ($P = 0.038$ and $P = 0.041$, one-way ANOVA, Tukey's *post hoc* test).

During phase II of the HVR, the increases in frequency and \int PNA were not significantly different between the three groups. Frequency was 1.16 ± 0.07 , 1.15 ± 0.04 and 0.97 ± 0.04 , and \int PNA was 1.28 ± 0.04 , 1.29 ± 0.08 and 1.17 ± 0.04 for naïve, viral control and TeLC expressing rats, respectively. Ventilatory output, however, was significantly lower in the TeLC expressing rats (1.12 ± 0.04) compared to naïve (1.49 ± 0.09) and eGFP expressing rats (1.48 ± 0.09) ($P = 0.024$, $P = 0.048$, respectively, one-way ANOVA, Tukey's *post hoc* test). Also, despite a modest elevation in the baseline mean arterial

pressure of the viral control group compared to the naïve control and TeLC expressing rats, the drop in blood pressure during phase II relative to baseline was the same in all groups. These data indicate that the vesicular release of gliotransmitters by preBötC astrocytes contributes to the enhanced ventilatory activity in both phases of the HVR.

Postmortem analysis of serial 50 μ m transverse brainstem sections from rats expressing eGFP and TeLC in medullary astrocytes revealed the extent of viral expression across the ventral respiratory column (VRC) (Fig. 4A). Viral expression was similar in both groups. It was strongest at the level of the preBötC where the injection pipette tracts were visible. The injection sites were located ~ 750 – 850 μ m caudal to the caudal border of the facial nucleus at the same level as anatomical markers of the preBötC (lateral loop of the principal subnucleus of the inferior olive and the semi-compact division of nucleus ambiguus, just caudal to its compact formation (Paxinos & Watson, 2007; Ruangkittisakul

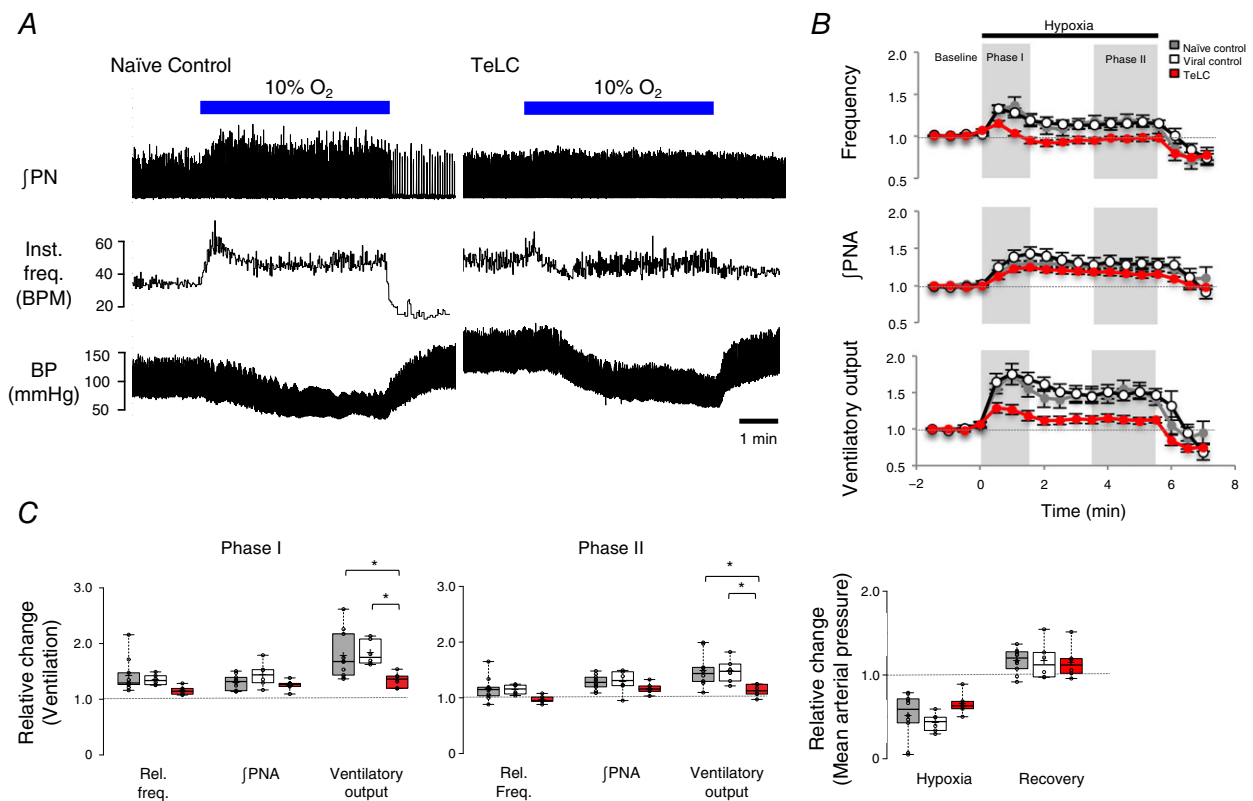


Figure 3. Expression of tetanus toxin light chain (TeLC) protein in medullary astrocytes attenuates the hypoxic ventilatory response

A, representative recordings obtained in naïve control and TeLC expressing rats showing changes in \int PN, instantaneous frequency (inst. freq., breaths min^{-1}) and blood pressure during 5.5 min of exposure to 10% O₂. B, time course of relative frequency, \int PNA and ventilatory output (frequency \times \int PNA) calculated for the three groups: naïve controls ($n = 10$), viral controls ($n = 6$) expressing eGFP in astroglia, and rats expressing eGFP and TeLC in astroglia ($n = 6$). Phases I and II of the HVR are shaded in grey. C, box plots comparing phase I and II parameters across the three groups. An asterisk (*) indicates a significant difference between means ($P < 0.05$, one-way ANOVA, Tukey's *post hoc* test).

et al. 2008). The strongest viral expression also overlapped with the site along the VRC with the highest density of NK1 receptor immunolabelling (Fig. 4B), an established marker of the preBötC (Gray *et al.* 1999; Guyenet & Wang, 2001; Guyenet *et al.* 2002). Viral expression dropped off substantially 500 μm rostral and caudal to the injection site centered in the preBötC (Fig. 4A).

The morphology of all eGFP and TeLC-expressing cells was consistent with astrocytic targeting (Gourine *et al.* 2010; Angelova *et al.* 2015). The efficacy of our viral vectors in transfecting medullary astrocytes has been demonstrated previously (Liu *et al.* 2008; Gourine *et al.* 2010; Tang *et al.* 2014). To further ensure the specificity and to determine whether TeLC is expressed in preBötC

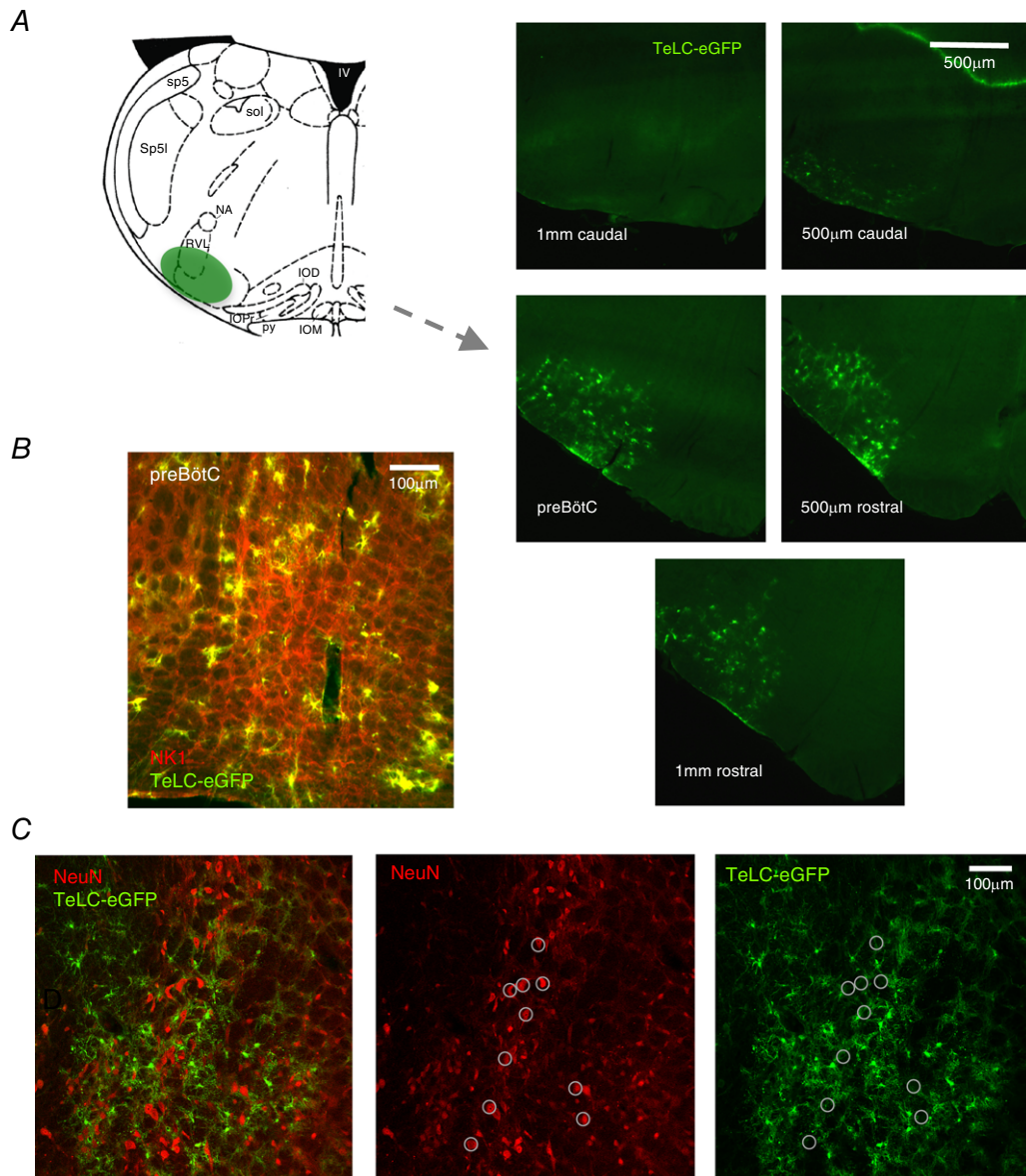


Figure 4. Viral expression was centered at the level of the preBötC and limited to astrocytes

A, schematic showing relative location of peak viral expression with respect to the preBötC in adult rats targeted with AVV-sGFAP-eGFP-TeLC. Inferior olive dorsal (IOD), inferior olive medial (IOM), inferior olive principal (IOP), fourth ventricle (IV), nucleus ambiguus (NA), pyramidal tract (PY), rostral ventrolateral medulla (RVL), spinal trigeminal tract (Sp5), spinal trigeminal interpolar (Sp5l) and solitary tract (Sol). Viral expression was centered in the preBötC and dropped off substantially 500 μm rostral and caudal to the injection site that was centered in the preBötC. B, region expressing TeLC-eGFP adenovirus is centered in the region containing a high density of NK1 receptor expressing neurons. C, double-labelling of cells with the neuronal marker NeuN and the glial specific adenovirus, detected via eGFP, was not detected. Ten NeuN labelled cells are circled to facilitate comparison between images.

neurons, we examined 253 transduced cells from three sections from three different animals for co-localization of eGFP expression with the immunoreactivity for a neuron specific marker NeuN. A representative example of eGFP and NeuN immunostaining and their overlay is shown in Fig. 4C. Ten NeuN labelled cells are circled to facilitate comparison. None of the NeuN labelled cells were transduced to express eGFP.

P2Y₁ receptor activation in the preBötC increases respiratory frequency in adult rats *in vivo*

The previous experiments using TeLC expression to block astroglial vesicular release did not identify the gliotransmitter(s) that excites the preBötC network. Substantial evidence, both *in vivo* (Gourine *et al.* 2005; Angelova *et al.* 2015) and *in vitro* (Lorier *et al.* 2004, 2007), points to the involvement of ATP. The next objective was to assess whether P2Y₁ receptors mediate the actions of ATP in the preBötC *in vivo*, as shown in Fig. 1 (iii). We therefore tested whether local, unilateral injection of the P2Y₁ receptor agonist, MRS 2365 (1 mM, *n* = 8) into the preBötC of anaesthetized, vagotomized spontaneously-breathing adult rats increases respiratory frequency.

The preBötC was functionally identified based on the stereotypical response to a microinjection of DLH (10 mM) that comprises a rapid-onset increase in inspiratory frequency and decrease in burst amplitude (Monnier *et al.* 2003), as shown in Fig. 5A. The excitatory effect of DLH was limited to a relatively small area. Injections 200 μm rostral to the preBötC (presumably in the BötC) reduced the inspiratory frequency (Fig. 5B), whereas injections 300 μm caudal had no effect on breathing (Fig. 5C).

A typical response of MRS2365 injection into the preBötC is shown in Fig. 6A. This recording, its corresponding time course (Fig. 6B) and group data (Fig. 6C) show that MRS 2365 microinjections into the preBötC *in vivo* significantly increased respiratory frequency to 1.44 ± 0.09 of the control ($P = 0.0013$). V_T decreased to 0.60 ± 0.09 of the control ($P = 0.0054$). The amplitude of \int DIA EMG and \int GG EMG (not shown) inspiratory bursts decreased similarly to 0.60 ± 0.10 ($P = 0.0049$) and 0.60 ± 0.05 ($P = 0.0002$) of the control, respectively (Fig. 6C). The increase in frequency and decrease in V_T offset each other such that minute ventilation (\dot{V}_E) was not significantly affected by P2Y₁ receptor activation, as expected in an actively breathing animal with intact chemoreceptor feedback mechanisms. Parallel decreases in diaphragm and GG EMG suggest a decrease in central drive. However, we cannot exclude the possibility that the decrease in V_T reflects an increase in airway resistance because GG EMG amplitude decreased. Nevertheless, the main result is that MRS 2365 administration in the preBötC *in vivo* evokes an increase

in respiratory frequency. Control (saline) injections into the same brainstem sites had no significant effect on the respiratory frequency, V_T or \dot{V}_E .

Histological analysis of brainstem sections confirmed the functional DLH mapping. The fluorescent microspheres that marked the MRS 2365 injection sites were localized in a region corresponding to the preBötC based on anatomical criteria and the relationship to NK1 receptor immunolabelling as described above (Fig. 6D). Injection sites are mapped onto a schematic (Fig. 6D).

Adenosine injection into the preBötC has no effect on ventilation in adult rats *in vivo*

Degradation of extracellular ATP into adenosine can inhibit respiratory activity, although sites, mechanisms and the effects of adenosine appear to be species- and age-dependent. In rats, the adenosine-mediated inhibition

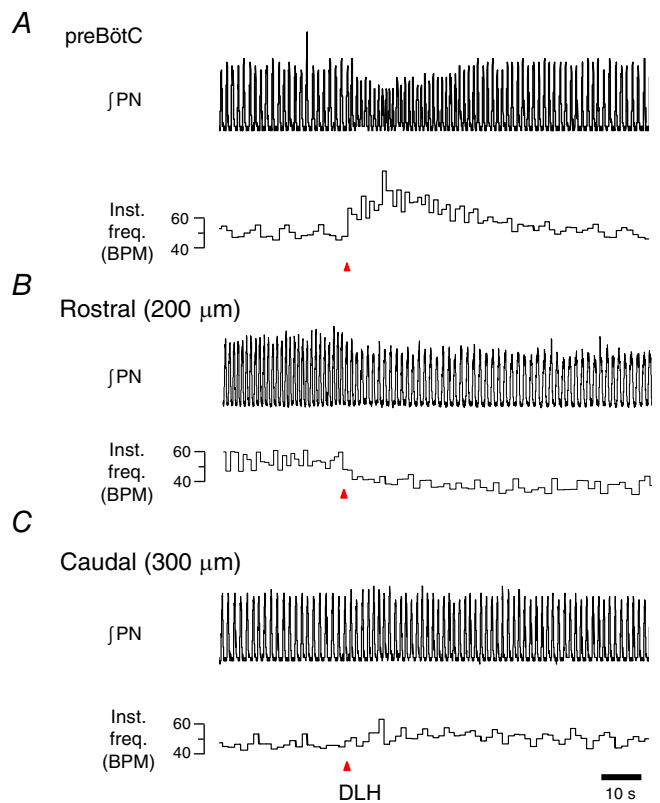


Figure 5. Functional identification of preBötC via microinjections of DLH

Unilateral injection of DLH (10 mM) into the VLM of urethane-anaesthetized, paralysed adult rats when measuring instantaneous respiratory frequency (inst. freq., breaths min⁻¹) from \int PN. A, unilateral injection of DLH into the preBötC produces a robust increase in respiratory frequency. B, injection of DLH 200 μm rostral to the preBötC (presumably in the BötC) reduced the inspiratory frequency. C, DLH injection 300 μm caudal to the preBötC had minimal effect on inspiratory rhythm.

of the preBötC activity is completely blocked by the A1 receptor antagonist DPCPX and disappears by postnatal day 2–3. In mouse, it is also A1 receptor mediated but lasts beyond postnatal day 3 (Huxtable *et al.* 2009; Zwicker *et al.* 2011). To determine whether the generation of adenosine from hydrolysed ATP could have a confounding influence on responses evoked by ATP released by preBötC astrocytes in adult rats, we microinjected adenosine (500 nl, 500 μM) unilaterally into the preBötC of adult, anaesthetized, vagotomized rats. The representative traces and group data (Fig. 7A and C) show that injections of adenosine had no significant effect on ventilation. Frequency, V_T and \dot{V}_E were 1.09 ± 0.03 , 1.02 ± 0.01 and 1.09 ± 0.02 of the control, respectively ($n = 7$, paired t test $P > 0.05$). Responses elicited by DLH delivery into the same brainstem sites confirmed that the injections were placed within the preBötC (Fig. 7C). DLH caused a significant and rapid 1.36 ± 0.05 -fold ($P = 0.004$) increase in frequency and parallel decrease in V_T to 0.67 ± 0.04 of

the control ($P = 0.002$) (Fig. 7C). Fluorescence-marked adenosine injection sites mapped to the preBötC based on anatomical landmarks (Fig. 7D). Figure 7E shows a high magnification fluorescence image in which fluorescent microspheres that mark the injection site are in a region of strong NK1 receptor immunoreactivity.

P2Y₁ receptor blockade in the preBötC of adult rats increases the secondary hypoxic respiratory depression

Given that ATP released in the ventral respiratory column during hypoxia appears to counteract the secondary respiratory depression (Gourine *et al.* 2005), and that ATP evokes P2Y₁ receptor mediated increases in respiratory activity by acting within the preBötC *in vitro* (Lorier *et al.* 2007) and *in vivo* (Fig. 6), we tested the hypothesis that the secondary hypoxic depression is reduced by ATP-induced activation of P2Y₁ receptors in the preBötC,

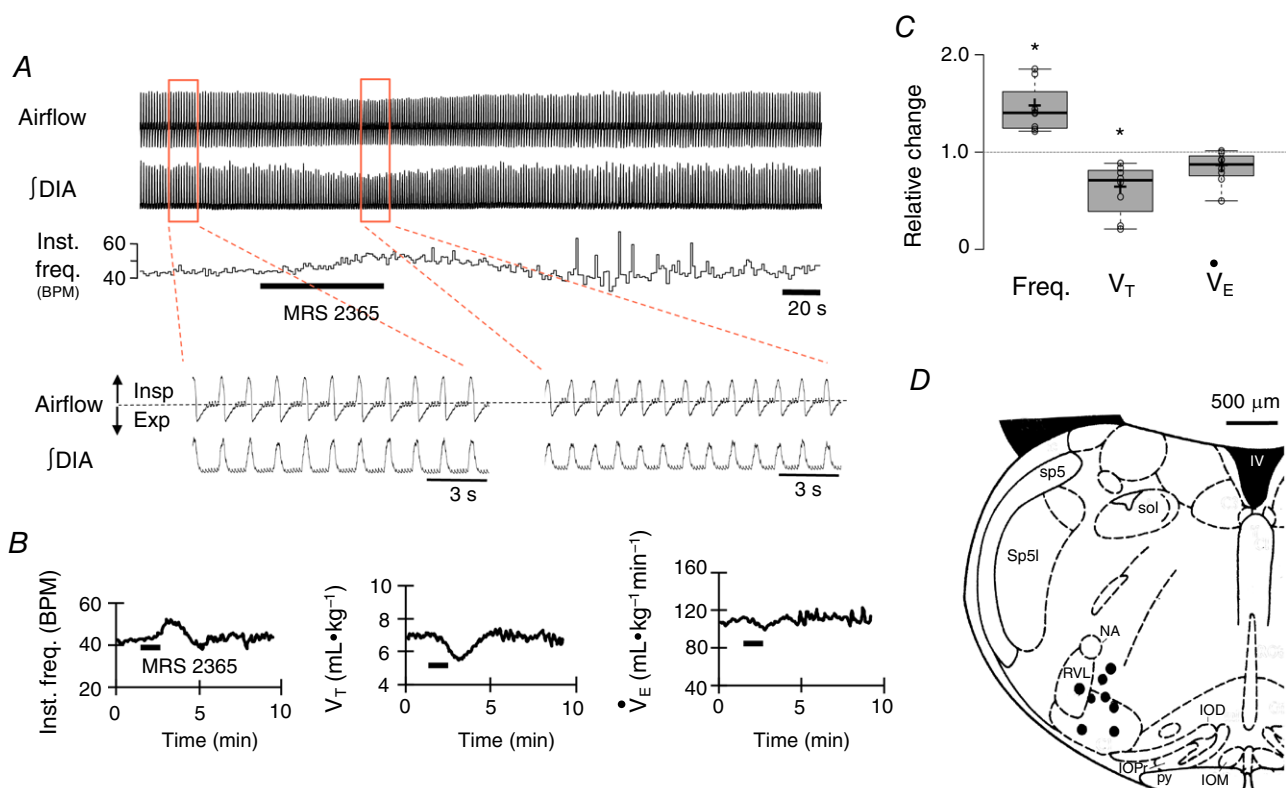


Figure 6. Activation of P2Y₁ receptors in the preBötC of adult rat *in vivo* with MRS 2365 (1 mm) evokes an increase in respiratory frequency and a decrease in tidal volume (V_T)

A, airflow and DIA EMG recordings show the response of an adult anaesthetized vagotomized rat to unilateral injection of MRS 2365 (1 mm, 200 nl) into the preBötC. B, time course of instantaneous frequency (inst. freq., breaths min^{-1}), V_T and minute ventilation (\dot{V}_E) responses evoked by a single injection of MRS 2365. C, group data ($n = 8$) illustrating the change in frequency, V_T and \dot{V}_E relative to control (*significant different from predrug control values, $P < 0.05$, paired t test). D, schematic showing eight injection sites. Inferior olive dorsal (IOD), inferior olive medial (IOM), inferior olive principal (IOP), fourth ventricle (IV), nucleus ambiguus (NA), pyramidal tract (PY), rostral ventrolateral medulla (RVL), spinal trigeminal (Sp5), spinal trigeminal interpolar (Sp5I) and solitary tract (Sol).

as shown in Fig. 1 (iii). We compared the HVRs of adult, urethane-anaesthetized, paralysed, mechanically ventilated and vagotomized rats following unilateral microinjections of vehicle (0.2 μ l HEPES buffer) or the P2Y₁ receptor antagonist, MRS 2279 (0.2 μ l, 500 μ M) into the preBötC, 2 min prior to the onset of hypoxia. \int PN was monitored as an index of central respiratory drive for 2 min in normoxia (30% O₂–70% N₂), 5 min in hypoxia (10% O₂–90% N₂) and then during the return to normoxia. Vehicle and MRS 2279 hypoxia trials were separated by 1 h to ensure that the rats had fully recovered from the first hypoxic challenge. Representative recordings of \int PN in Fig. 8 show the hypoxic responses of one animal after vehicle and MRS 2279 microinjections into the preBötC.

Blockade of P2Y₁ receptors with MRS 2279 had no effect on baseline inspiratory frequency, phrenic burst amplitude or ventilatory output. Frequency

was 45.7 ± 2.4 breaths min⁻¹ at baseline and 45.6 ± 2.5 breaths min⁻¹ after MRS 2279 injection (i.e. it remained at $99.8 \pm 1.6\%$ of baseline). Similarly, phrenic burst amplitude and ventilatory output remained at $99.4 \pm 2.1\%$ and $99.3 \pm 3.6\%$ of baseline after unilateral microinjections of MRS 2279 into the preBötC.

Blockade of P2Y₁ receptors with MRS 2279 also had no effect on the initial phase I of the HVR. In the control (after microinjections of the vehicle) hypoxia trials, frequency, burst amplitude and ventilatory output increased in phase I to levels that were 1.42 ± 0.08 , 1.52 ± 0.11 , and 1.83 ± 0.23 -fold greater than baseline, respectively. In MRS 2279, hypoxia evoked phase I increases in frequency, burst amplitude and ventilatory output that were 1.17 ± 0.06 , 1.23 ± 0.06 and 1.36 ± 0.11 of baseline. Only the change in burst amplitude was significantly reduced compared to control during phase I ($P = 0.038$, paired t test, $n = 6$).

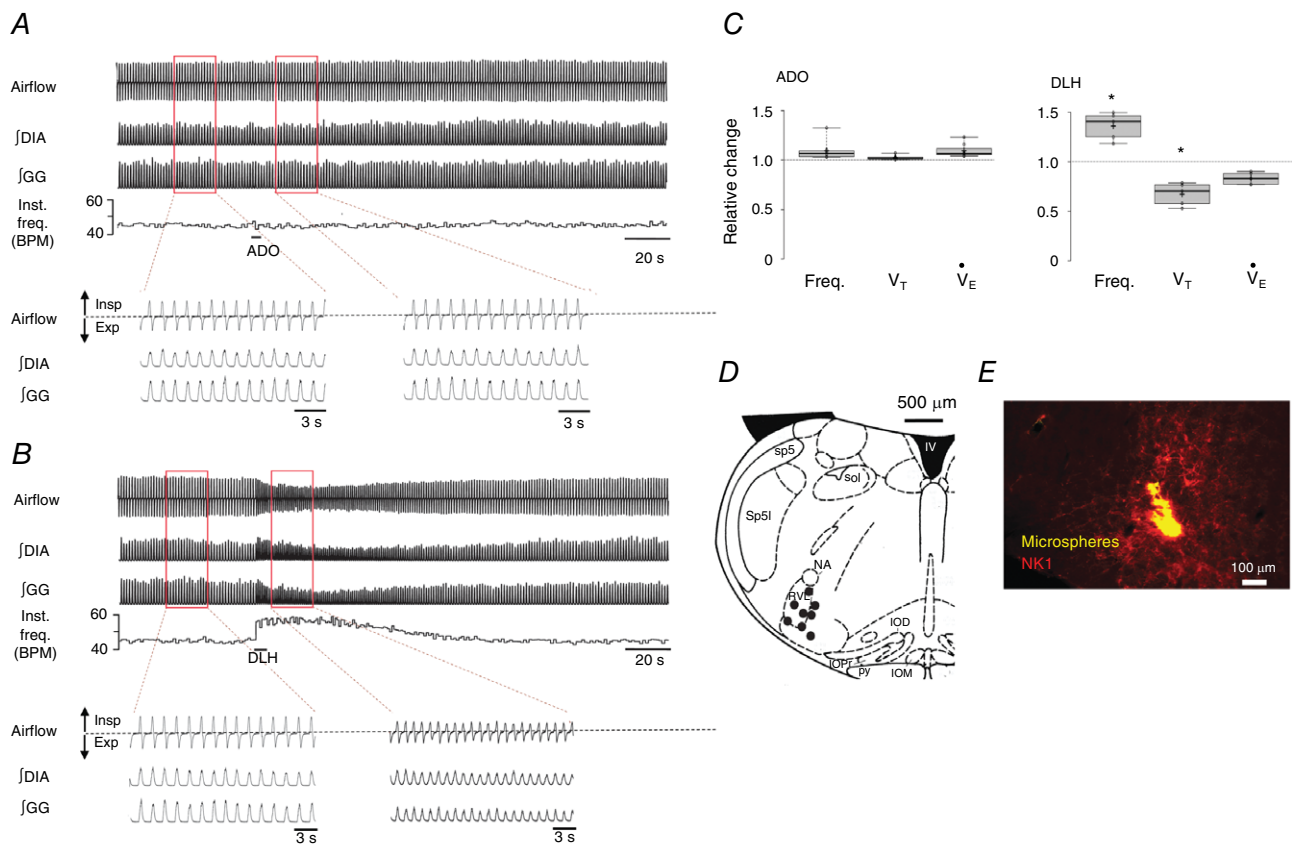


Figure 7. Adenosine (500 μ m) microinjected into the preBötC of adult rat *in vivo* has no effect on respiratory frequency or tidal volume (V_T)

A, airflow, DIA and genioglossus (GG) EMG recordings show the response of an adult anaesthetized vagotomized rat to unilateral injection of adenosine into the preBötC. **B**, airflow, diaphragm (DIA) and genioglossus (GG) EMG recordings show the response of an adult anaesthetized vagotomized rat to the injection of DLH (1 mM) into the preBötC. **C**, group data illustrating the change in frequency and V_T relative to control ($n = 8$) (*significant difference from predrug controls values, $P < 0.05$, paired t test). **D**, schematic showing eight injection sites in relation to inferior olive dorsal (IOD), inferior olive medial (IOM), inferior olive principal (IOP), fourth ventricle (IV), nucleus ambiguus (NA), pyramidal tract (PY), rostral ventrolateral medulla (RVL), spinal trigeminal tract (Sp5), spinal trigeminal interpolar (Sp5l) and solitary tract (Sol). **E**, tissue section showing injection site marked with fluorescent microspheres (yellow). PreBötC neurons (NK1⁺) are present in the region of the injection site.

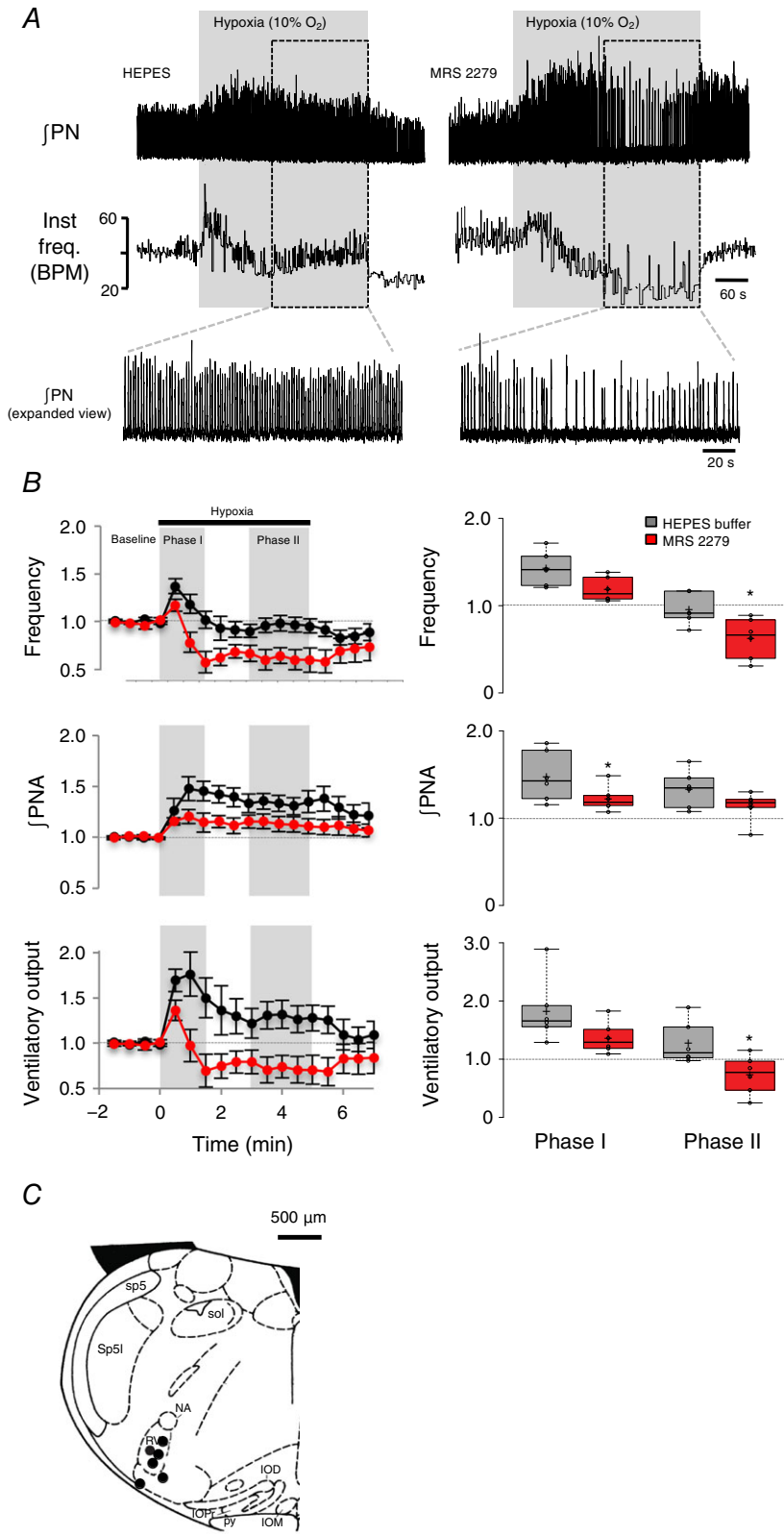


Figure 8. Unilateral inhibition of P2Y₁ receptors in the preBötC of adult paralysed rats *in vivo* with MRS 2279 increases the secondary hypoxic respiratory depression

A, representative traces showing changes in \dot{V}_{PN} and instantaneous frequency (inst. freq., breaths min^{-1}) evoked by exposure to 5 min of 10% O_2 following injection of vehicle (HEPES) or MRS 2279 into the preBötC. **B**, left: time courses of relative frequency, \dot{V}_{PNA} and ventilatory output (frequency $\times \dot{V}_{PNA}$) calculated before and after injection of MRS 2279 ($n = 6$). Phases I and II of the HVR are shaded in grey. Right: comparisons of phase I and II parameters between vehicle and MRS 2279 responses [*significant difference between control (HEPES) and MRS 2279 trials, $P < 0.5$, paired t test]. **C**, schematic showing six injection sites. Inferior olive dorsal (IOD), inferior olive medial (IOM), inferior olive principal (IOP), fourth ventricle (IV), nucleus ambiguus (NA), pyramidal tract (PY), rostral ventrolateral medulla (RVL), spinal trigeminal tract (Sp5), spinal trigeminal interpolar (Sp5l) and solitary tract (Sol).

By contrast, MRS 2279 significantly reduced the respiratory activity during phase II of the HVR. In the vehicle trials, during phase II, frequency fell to 0.95 ± 0.07 of baseline and burst amplitude remained elevated at 1.34 ± 0.09 of baseline such that ventilatory output remained above the baseline level recorded during normoxia (1.28 ± 0.15). After MRS 2279 application, frequency and \dot{V}_E fell to the levels significantly below that seen in the vehicle controls and below baseline. Frequency fell to 0.62 ± 0.10 ($P = 0.045$, paired t test, $n = 6$) of the control, whereas ventilatory output was 0.73 ± 0.14 ($P = 0.027$, paired t test, $n = 6$) of baseline. Group data are summarized in Fig. 8B. Injection sites marked with fluorescent microspheres localized to the preBötC anatomically and based on the pattern of NK1 receptor immunolabelling (Fig. 8C).

To ensure that the greater hypoxic depression following MRS 2279 microinjections into the preBötC was not a result of time-dependent changes in the HVR with repeated hypoxic exposures, we performed a control series of experiments in which the hypoxia protocol was repeated at an interval of 1 h but the first and second hypoxic challenges were preceded by a vehicle injection. The frequency, \int PNA and ventilatory output responses to the two consecutive hypoxic responses were not significantly different ($n = 5$) (Fig. 9). Comparison of the second hypoxia response in this time control series with the hypoxia response in MRS 2279 from the previous series (i.e. unpaired data) also showed that, during phase II, MRS 2279 caused a significant reduction in both frequency and ventilatory output ($P = 0.01$ and 0.03 , respectively, independent samples t test).

Increases in $[Ca^{2+}]_i$ contribute to the excitatory actions of P2Y₁ receptor activation on the inspiratory rhythm generated by the preBötC

Having shown that ATP acting at P2Y₁ receptors in the preBötC contributes to the HVR *in vivo*, we next used rhythmic brainstem slice preparations to study the signalling pathways via which P2Y₁ receptor activation excites the preBötC network (Funk *et al.* 1997; Lorier *et al.* 2004, 2007, 2008; Huxtable *et al.* 2009; Zwicker *et al.* 2011). Note that, as a result of the limitations associated with using rhythmic medullary slices to explore mechanisms underlying homeostatic ventilatory responses to hypoxia (Funk & Greer, 2013), these studies do not examine responses to hypoxia/anoxia *in vitro*. Instead, our approach was to investigate mechanisms by which P2Y₁ receptor-mediated signalling pathways, as activated *in vivo* during hypoxia, modulate preBötC network activity. Analyses of recombinant P2Y₁ receptors and native P2Y₁ receptors in other brain regions indicate that responses depend on increases in $[Ca^{2+}]_i$ (Rajani *et al.* 2015). $[Ca^{2+}]_i$ -dependent pathways can increase

excitability by modulating the activity of multiple ion channels, as shown in Fig. 1 (iv) and (v). We therefore tested the hypothesis that increases in $[Ca^{2+}]_i$ are necessary for P2Y₁ receptor activation to increase inspiratory frequency. We compared the responses of the preBötC network to local MRS 2365 administered after local application of vehicle or the Ca²⁺ chelator, EGTA-AM (1 mM). We used MRS 2365 rather than ATP because the frequency effect is mediated by P2Y₁ receptors and also because MRS 2365 avoids the confounding inhibitory actions on neonatal networks as a result of the adenosine that is generated from the degradation of ATP by endogenous ectonucleotidases. Vehicle and EGTA-AM (1 mM) were locally applied to the preBötC for 5 min (5 s on, 5 s off), prior to local application of MRS 2365 (10 s, 100 μ M). EGTA-AM alone caused a significant, $30.6 \pm 6.8\%$ reduction in baseline inspiratory frequency from 12.2 ± 1.1 to 8.3 ± 0.7 breaths min^{-1} . ($n = 6$, $P = 0.007$, paired t test). As shown for a single slice preparation and group data in Fig. 10A, EGTA-AM also significantly reduced the MRS 2365-induced response from a 2.1 ± 0.14 -fold increase in the control to a 1.5 ± 0.08 -fold increase in EGTA-AM (i.e. EGTA reduced the magnitude of the MRS 2365 frequency increase by $59 \pm 12\%$) ($n = 6$, $P = 0.0047$, paired t test). Reporting the MRS 2365-evoked frequency relative to baseline values may even underestimate the effects of EGTA. Under control conditions, MRS 2365 caused the frequency to increase from 12.2 ± 1.1 to 25.1 ± 1.8 cycles min^{-1} , which is an increase of ~ 13 cycles min^{-1} . By contrast, in EGTA-AM, MRS 2365 caused the frequency to increase from 8.3 ± 0.7 to 12.5 ± 1.2 cycles min^{-1} , which is increase of ~ 4 cycles min^{-1} .

To assess whether the increase in intracellular $[Ca^{2+}]_i$ that contributes to the P2Y₁ receptor evoked frequency increase is derived from intracellular sources, we next compared control MRS 2365 responses evoked after vehicle (DMSO 0.2%) application with those evoked after local application of thapsigargin (200 μ M), a SERCA inhibitor that depletes intracellular calcium stores, to the preBötC. Similar to EGTA-AM, the target of thapsigargin is intracellular, although thapsigargin is not designed with an AM ester to facilitate diffusion across membranes. Thus, additional time was allowed for thapsigargin to diffuse into the tissue and cross cell membranes. MRS 2365 applications were preceded by 30 min of pre-application (5 s on, 5 s off) of vehicle or thapsigargin. The responses of a single preparation and group data are shown in Fig. 10C and D, respectively. First, application of thapsigargin for 30 min had no effect on the baseline inspiratory-related rhythm. Frequency was 13.4 ± 0.6 cycles min^{-1} in the control and 14.2 ± 1.4 cycles min^{-1} 30 min after thapsigargin application. By contrast, 30 min of thapsigargin application reduced the MRS 2365 evoked frequency increase from a 2.59 ± 0.15 -fold increase to

1.90 ± 0.21 ($n = 6$, $P = 0.007$, paired t test). A series of control experiments comparing the response of MRS 2365 before and after 30 min of local application of DMSO (0.2%) established that the thapsigargin-mediated inhibition was not a result of the actions of the vehicle but rather the effect of SERCA inhibition. Vehicle application

for 30 min did not affect the MRS 2365 response ($n = 5$, $P > 0.05$, paired t test). A different SERCA blocker, CPA ($100 \mu\text{M}$), was tested using a similar protocol except that the vehicle contained 0.1% DMSO. Baseline inspiratory frequency was similar under control conditions (12.1 ± 2.5 cycles min^{-1}) and after 45 min

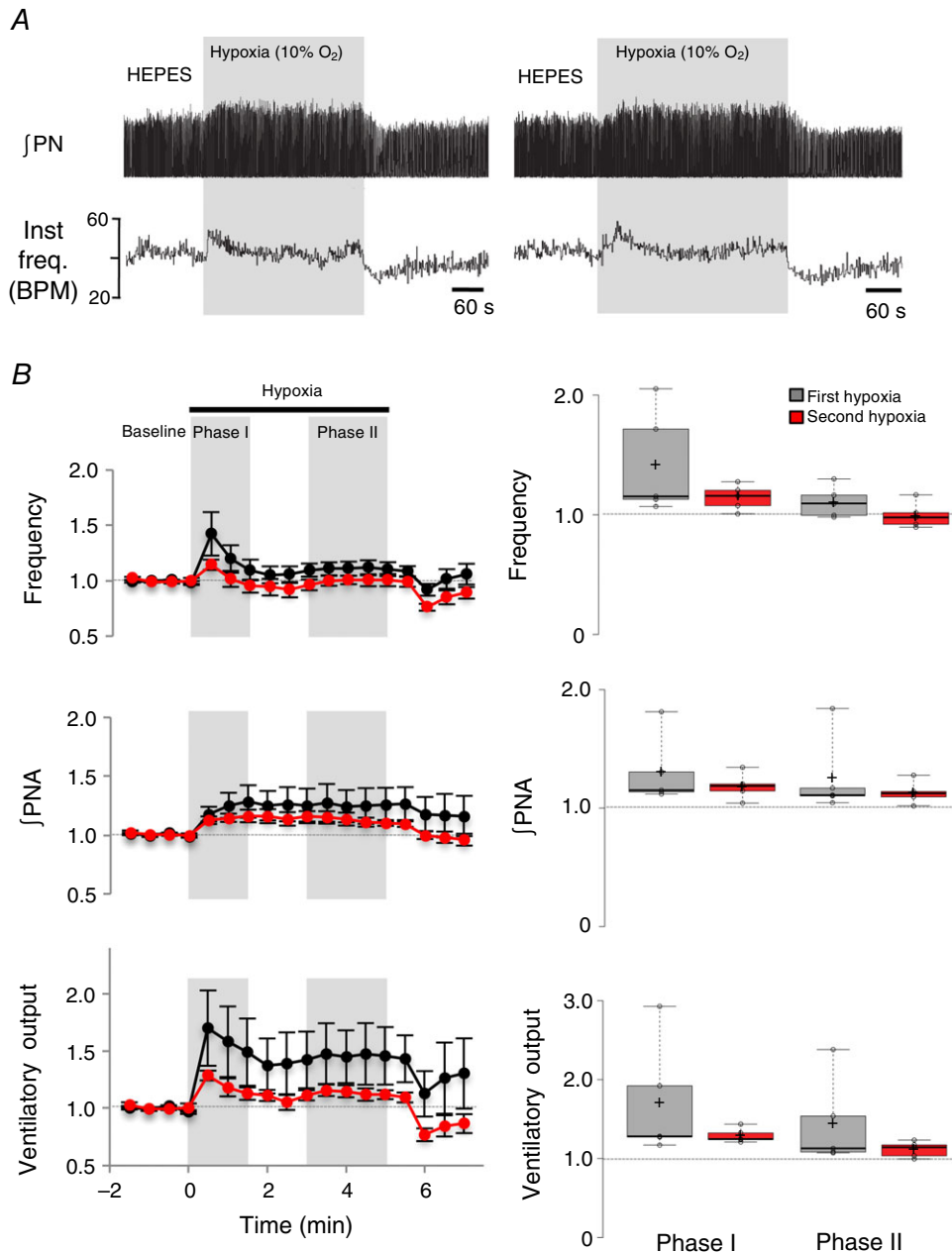


Figure 9. The hypoxic ventilatory response does not change with repeated exposure; time-matched controls

A, representative traces from the same animal showing changes in \dot{V}_{PN} and instantaneous frequency (inst. freq., breaths min^{-1}) during two consecutive hypoxic exposures (1 h apart) following stereotaxic injection of vehicle (Hepes) into the preBötC. *B*, left: time courses of relative frequency, \dot{V}_{PNA} and ventilatory output (frequency $\times \dot{V}_{\text{PNA}}$) calculated before and after injection of MRS 2279 ($n = 6$). Phases I and II of the HVR are shaded in grey. Right: box plots comparing these same parameters during phases I and II of the HVR during consecutive exposures to hypoxia under control conditions (i.e. after Hepes injection).

of CPA application (11.7 ± 1.3 cycles min^{-1}). Although CPA had no effect on baseline frequency, it reduced the MRS 2365-evoked frequency increase by $\sim 35\%$ from a peak of 2.80 ± 0.28 fold in vehicle to 1.82 ± 0.12 after 45 min of CPA ($n = 6$, $P = 0.040$, paired t test; data not shown).

P2Y₁ receptor activation increases [Ca²⁺]_i in preBötC inspiratory neurons and glia

The EGTA- and thapsigargin-induced reductions in the P2Y₁ receptor-evoked frequency increase indicate that increases in [Ca²⁺]_i are an important part of ATP-mediated excitatory signalling in the preBötC. These data, however, do not establish whether the ATP-evoked frequency increase depends on an increase in neuronal [Ca²⁺]_i (Fig. 1 iv), glial [Ca²⁺]_i (Fig. 1 ii) or both. To gain insight into the cells that mediate the network excitation, we tested whether inspiratory neurons and glia in the preBötC respond to ATP with an increase in [Ca²⁺]_i.

To test neuronal sensitivity, we loaded the preBötC of rhythmic slices with the Ca²⁺-sensitive dye, Fluo-4.

Fluo-4 fluorescence and XII inspiratory nerve activity were recorded during local application of MRS 2365 ($100 \mu\text{M}$) to the preBötC. Inspiratory neurons were identified by rhythmic increases in the Fluo-4 signal in phase with the rhythm recorded from the XII nerve (Fig. 11). Five such neurons are marked with arrows in Fig. 11A and their baseline, inspiratory-related oscillations in [Ca²⁺]_i are apparent in the recordings of fluorescence intensity (Fig. 11B). Local application of MRS 2365 ($100 \mu\text{M}$) near the surface of the slice evoked significant increases in preBötC frequency and the Fluo-4 signal in all five inspiratory neurons imaged in this slice (Fig. 11B). Group data taken from 18 inspiratory neurons in five slices showed a similar 1.53 ± 0.06 -fold increase in the fluo-4 [Ca²⁺]_i signal (Fig. 11C) ($n = 18$ from five slices, $P < 0.0001$, paired t test).

To test whether the MRS 2365-evoked increase in [Ca²⁺]_i derives from intracellular sources, we compared the MRS 2365 response in control (1 min, $10 \mu\text{M}$) with that evoked after the SERCA blocker thapsigargin ($100 \mu\text{M}$) or CPA ($100 \mu\text{M}$) was bath applied for 30 min. To account for any changes to the MRS 2365-evoked fluorescence

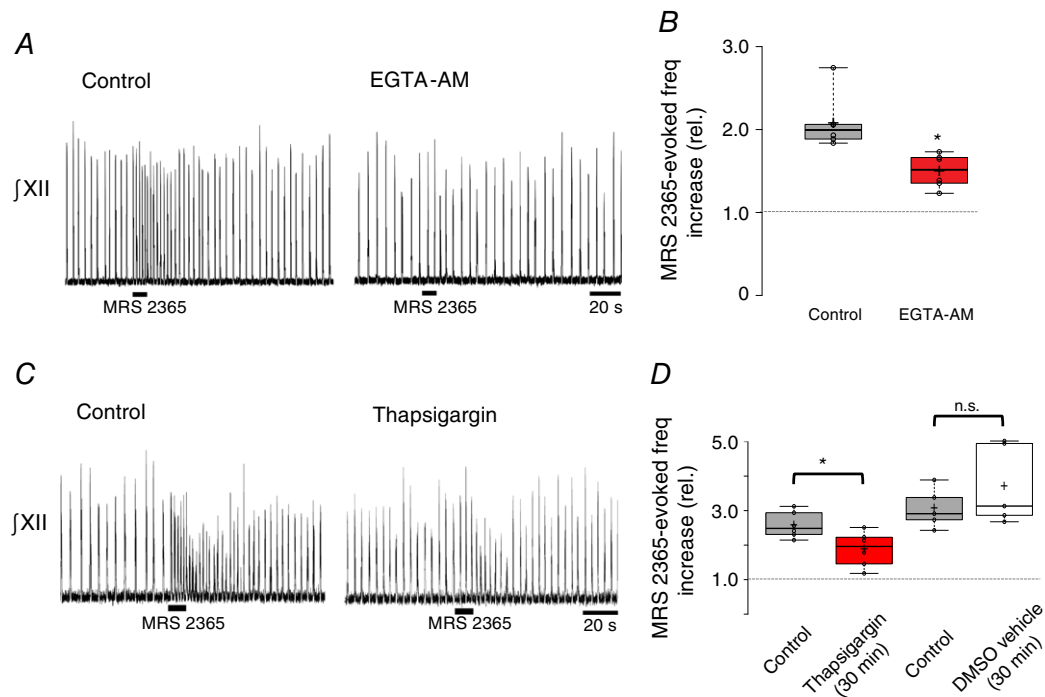


Figure 10. Increases in [Ca²⁺]_i contribute to the P2Y₁ receptor mediated frequency increase *in vitro*

A, representative traces of integrated hypoglossal nerve output (JXII) evoked in response to P2Y₁ agonist MRS 2365 (10 s , $100 \mu\text{M}$) before and after the local application of the cell permeable calcium chelator EGTA-AM (1 mM) to the preBötC. B, box plot summarizing group data (*significant difference between means, $n = 6$; $P = 0.0047$, paired t test). C, representative traces JXII nerve output evoked in response to MRS 2365 (10 s , $100 \mu\text{M}$) in control and after local application of thapsigargin (30 min , $200 \mu\text{M}$). D, box plot of group data showing the effects of thapsigargin on the MRS 2365 evoked frequency increase (two left-most boxes, $n = 6$) and time-matched control experiments showing the effects of repeated vehicle injections (0.2% DMSO, $n = 5$) on the MRS 2365 response (* indicates significant difference between means, $P < 0.05$, paired t test).

as a result of photobleaching, two consecutive control MRS 2365 applications were applied 30 min apart. The second control MRS 2365 response was then followed by the application of thapsigargin or CPA for 30 min and another MRS 2365 application. Two inspiratory

neurons are marked in Fig. 11D, along with their Fluo-4 fluorescence signals in Fig. 11E. We compared the decrease in fluorescence that occurred between MRS 2365 control trial 1 and control trial 2 with the decrease observed between control trial 2 and the trial with SERCA

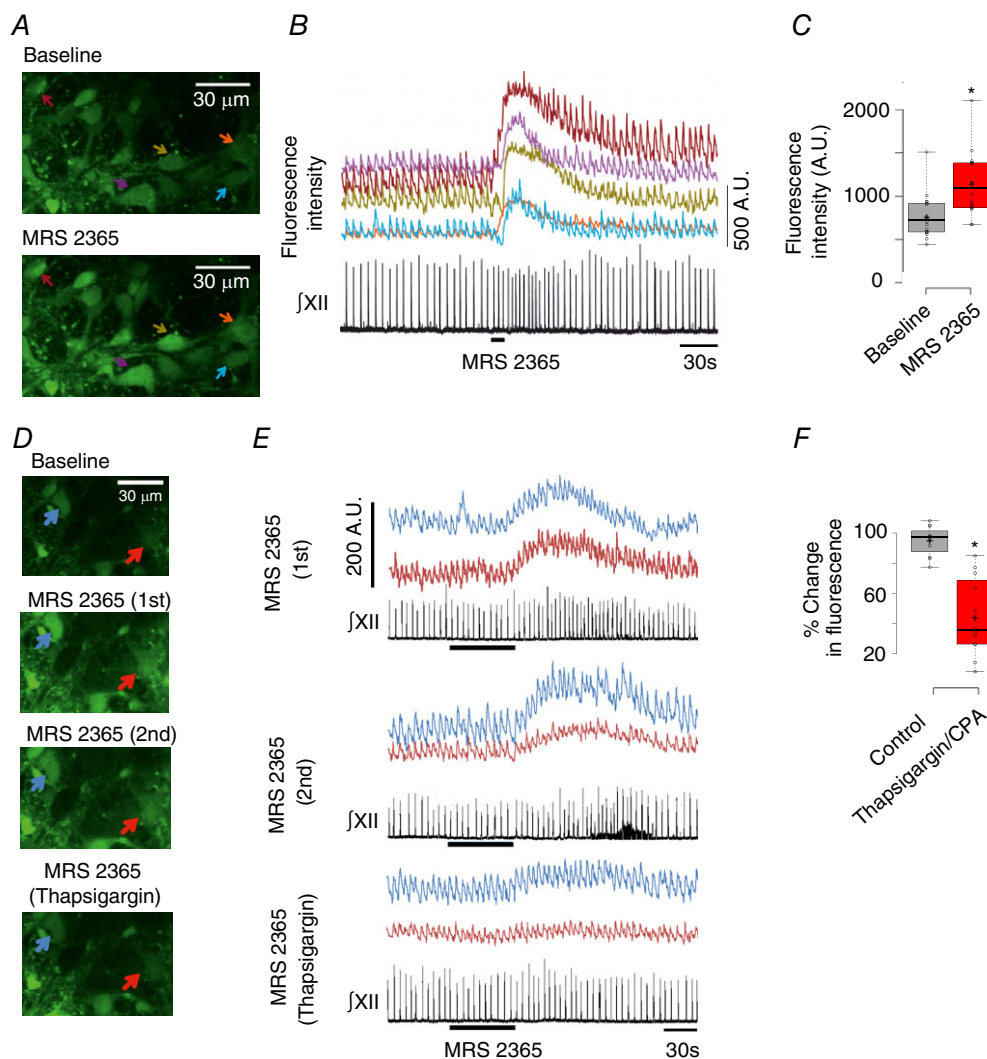


Figure 11. Activation of P2Y₁ receptors on preBötC inspiratory neurons *in vitro* evokes a thapsigargin-sensitive, increase in [Ca²⁺]_i;

A, multiphoton images of baseline Fluo-4 fluorescence indicating [Ca²⁺]_i in five inspiratory neurons at a single optical plain (top), inspiratory-related oscillations in [Ca²⁺]_i and the peak [Ca²⁺]_i increase evoked in response to locally applied MRS 2365 (100 μM, 10 s) (bottom) (B) [Ca²⁺]_i increases in the neurons of (A) are synchronous with \int XII and their responses to locally applied MRS 2365 (100 μM, 10 s). C, group data showing an increase of ~50% in peak Fluo-4 fluorescence in response to local application of MRS 2365 (100 μM, 10 s) over inspiratory preBötC neurons ($n = 18$, five slices; *significant difference between means, $P < 0.0001$, paired t test); AU, arbitrary units. D, multiphoton images of Fluo-4 Ca²⁺ fluorescence in two inspiratory neurons at a single optical plain at baseline (top), at the peak of two control MRS 2365-evoked (10 μM, 1 min, bath application) Ca²⁺ fluorescence responses (top middle, bottom middle), separated by 30 min intervals. The bottom image shows the response evoked by MRS 2365 after bath application of thapsigargin (100 μM, 30 min). E, traces of Fluo-4 Ca²⁺ fluorescence responses evoked by MRS 2365 in the same neurons shown in (D). F, box plot of group data comparing the decrease in peak MRS 2365-evoked Fluo-4 Ca²⁺ response that occurred between the second control MRS 2365 response and the MRS 2365 response in thapsigargin (or CPA) ($n = 12$, five slices; *significant difference between means, $P < 0.0001$, paired t test).

blockers. Thapsigargin ($n = 8$ neurons, four slices) and CPA ($n = 4$ neurons, one slice) had similar effects on the MRS 2365 evoked increase in Ca²⁺ dye fluorescence, and so these data were pooled ($n = 12$ neurons, five slices). There was only a small decrease in Ca²⁺ dye fluorescence between the two control trials; trial 2 response was $95.0 \pm 2.7\%$ of the first. In marked contrast, the reduction in the Ca²⁺ dye fluorescence response between the MRS 2365/thapsigargin trial and control trial 2 was significantly greater than the reduction in the MRS 2365 fluorescence response that occurred between control trials 1 and 2. In thapsigargin/CPA, the MRS 2365 evoked fluorescence increase was only $43.9 \pm 7.3\%$ of the control trial 2 ($n = 12$ neurons, five slices, $P < 0.0001$, paired t test) (Fig. 11F).

Although the preBötC is the critical site for inspiratory rhythm generation, it contains multiple subtypes of inspiratory-related neurons that can be differentiated based on embryonic origin (Dbx1), peptide (SST) or peptide receptor (NK1, μ -opioid) expression, presence or absence of pacemaker properties and whether they are excitatory (glutamatergic) or inhibitory (GABAergic). The high sensitivity of the preBötC network to P2Y₁ receptor excitation suggests that there may be a specific excitatory, ATP-sensitive population of preBötC neurons that either generates rhythm or provides drive to rhythm-generating neurons. By contrast, if diverse excitatory and inhibitory preBötC inspiratory neurons are ubiquitously excited by ATP, one might predict a blunted network sensitivity to ATP. As an initial foray into this important question, we simply investigated whether all inspiratory modulated preBötC neurons are sensitive to P2Y₁ receptor activation. As above, we used Ca²⁺-imaging of Fluo4-loaded rhythmic slices, identified inspiratory neurons based on rhythmic Ca²⁺ oscillations in phase with XII nerve output and counted cells that did or did not respond to MRS 2365 with an increase in Ca²⁺ fluorescence. In these experiments, MRS 2365 was bath-applied to activate as many neurons as possible and to prevent false negatives that can occur with local application when the drug does not diffuse from the pipette to the neuron in question. Neurons were only counted as weak- or non-responders if there were other neurons in the same field of view that showed a strong response to MRS 2365. When all the data were grouped, 20 neurons from seven slices showed an average $30.8 \pm 6.8\%$ increase in fluorescence above baseline (data not shown). However, these 20 neurons could be divided into weak/non-responders and responders. Eight of the 20 neurons responded to MRS 2365 with an average increase in fluorescence of only $6.5 \pm 2.8\%$. The remaining 12 neurons were, on average, seven times more sensitive, responding with an average $47 \pm 10\%$ increase in fluorescence.

To explore the signalling pathways through which ATP excites preBötC glial cells, glia were isolated from preBötC

tissue punches and grown in culture using sorbitol in place of glucose as the metabolic substrate because only glia can utilize sorbitol. Cultures were loaded with Fluo-4-AM. Local application of ATP ($10 \mu\text{M}$, 10 s) evoked a 3.1 ± 0.2 -fold increase in Ca²⁺ dye-related fluorescence (Fig. 12), which we have shown previously is primarily mediated by P2Y₁ receptors (i.e., it is blocked by MRS 2279 but neither suramin, nor PPADS (Huxtable *et al.* 2010)). Images of baseline fluorescence, the peak ATP response in control and after bath application of the SERCA blocker, thapsigargin (50 nM , 30 min), are shown for a group of cultured glial cells in Fig. 12A, along with the time course of fluorescence changes for four of these cells in Fig. 12B. Bath application of thapsigargin almost blocked the ATP-evoked increase in Ca²⁺ related fluorescence, which rose to only 1.18 ± 0.03 of baseline (Fig. 12B) ($n = 54$ cells from four culture plates, each plate was from one animal; $P < 0.001$, paired t test).

ATP-induced excitation of preBötC neurons does not involve glia-derived glutamate

ATP (Angelova *et al.* 2015) and glutamate (Huxtable *et al.* 2010) are major gliotransmitters that are released from cultured preBötC glia in response to hypoxia or ATP, respectively. Therefore, we next examined the possibility that, during hypoxia, the autocrine/paracrine activation of astrocytes by ATP evokes additional gliotransmitter release, which could contribute to the HVR (Fig. 1, vi). We tested this indirectly by determining whether stimulation of astrocytes with exogenous ATP evokes glutamate-mediated excitation of inspiratory neurons. In rhythmic slices, we obtained whole-cell voltage clamp recordings from preBötC inspiratory neurons, identified by rhythmic synaptic inputs in phase with inspiratory-related bursts in the XII nerve. We then applied TTX ($0.5 \mu\text{M}$) to block action potential-dependent transmitter release and compared the neuronal response to locally applied ATP before and during application of glutamate receptor antagonists, CNQX ($10 \mu\text{M}$) and AP5 ($100 \mu\text{M}$)/MK-801 ($100 \mu\text{M}$) ($n = 8$ cells from eight slices). CNQX/AP5 was used in three of eight experiments, whereas CNQX/MK-801 was used in the other five. Data were pooled because the effects of AP5 and MK801 were the same. Because locally applied ATP can stimulate astrocytes and neurons, we predicted that, if glial-derived glutamate contributes to the neuronal ATP response, the ATP current would decrease in CNQX and AP5/MK-801. As a result of the potential for time-dependent reduction in the amplitude of ATP currents, data obtained in the CNQX and AP5/MK-801 protocol were compared with a time-matched control group that received repeated ATP injections at 15 min intervals. ATP currents are reported as a ratio of the difference between the ATP current amplitudes evoked in the first and second applications

divided by the first current. A value of zero indicates that the first and second ATP currents were the same. A negative value indicates the second response was smaller than the first and vice versa. Fig. 13A shows a representative voltage clamp recording from an inspiratory neuron and

currents evoked by ATP in control (pre-TTX, rhythmic inspiratory synaptic currents are present), after TTX and again after application of CNQX and AP5 (in the continued presence of TTX). The current traces and group data both indicate that there is no effect of glutamate

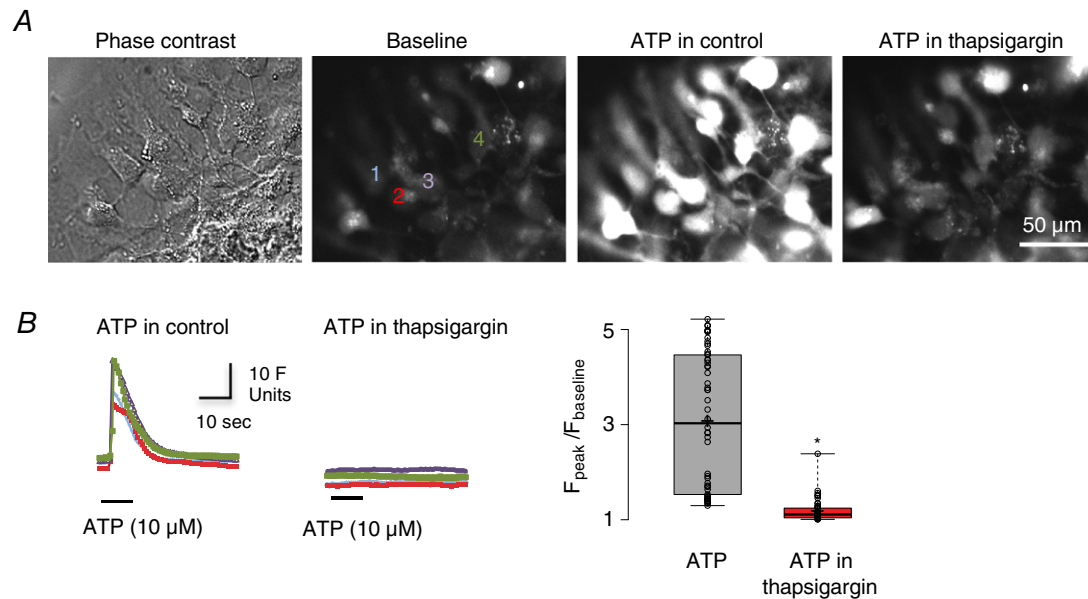


Figure 12. Responses of cultured preBötC glia to ATP are sensitive to depletion of intracellular calcium stores

A, images showing a phase contrast image of cultured glia (far left) and fluo-4 Ca^{2+} fluorescence under baseline conditions (middle-left), during local application of ATP ($10 \mu M$, 10 s) (middle-right) and during local application of ATP after pre-application of SERCA inhibitor thapsigargin (50 nM , 30 min) (far right). B, time course of ATP-evoked fluorescence changes measured from four regions of interest (numbered in A) in control (left) and after thapsigargin application (middle). Group data ($n = 54$ cells, from four culture plates, each plate was from one animal) showing relative changes in fluorescence ($F_{peak}/F_{baseline}$) in response to ATP and to ATP in the presence of thapsigargin (right) ($n = 54$ cells; *significant difference between means $P < 0.001$, paired t test).

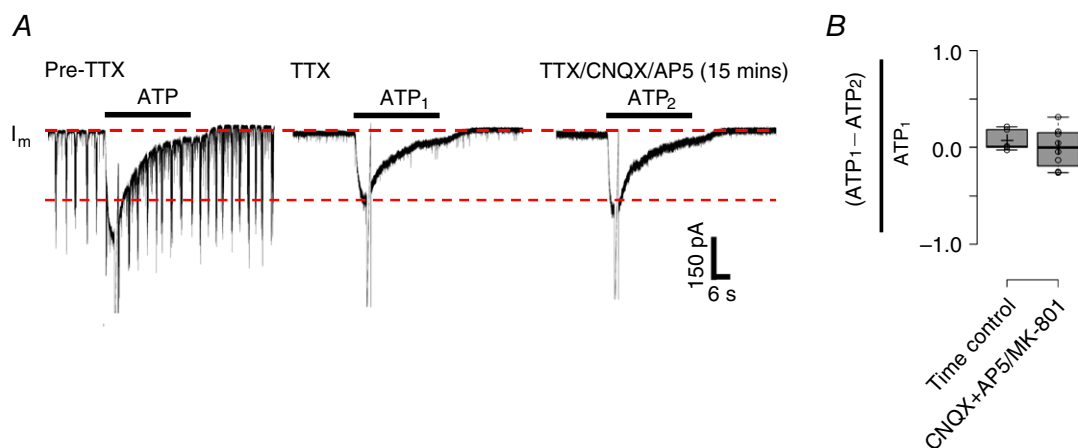


Figure 13. Effect of CNQX and AP5/MK-801 on ATP currents evoked in preBötC inspiratory neurons in TTX

A, representative traces showing an ATP current evoked in an inspiratory preBötC neuron in a rhythmic slice (note inspiratory synaptic currents pre-TTX), after TTX and again in TTX after bath application of CNQX ($10 \mu M$) and AP5 ($100 \mu M$). B, group data comparing the relative reduction in the ATP current that occurs with consecutive applications in a time matched-control group ($n = 6$ cells from six slices) with the reduction that was produced by CNQX+AP5/MK-801 group ($n = 8$ from eight slices).

receptor antagonism on the ATP current. The ATP current evoked in TTX plus CNQX+AP5/MK-801 groups was similar to that prior to addition of CNQX+AP5/MK-801 (e.g. it was $0.2 \pm 8.0\%$ smaller than following the first ATP application). In the time-control group, ATP currents decreased $6.4 \pm 4.7\%$ between the first and second applications. Similarly, CNQX+AP5/MK-801 had no effect on the reversal potential of the ATP-evoked current or the associated reduction in neuronal input resistance. Under control conditions (in TTX) the ATP current reversed at -26.5 ± 5.4 mV and was associated with a decrease in input resistance from 195 ± 40 M Ω to 148 ± 29 M Ω ($n = 8$) in ATP. In TTX/CNQX/AP5 (MK801), the ATP current reversed at -24.2 ± 5.9 mV and caused input resistance to decrease from a baseline of 186 ± 35 M Ω to 158 ± 35 M Ω in ATP ($n = 8$). We did not examine ATP-evoked ATP release from astrocytes because P2 receptor antagonists would block the initial ATP response.

Discussion

The biphasic ventilatory response of mammals to acute, moderate hypoxia comprises an initial, phase I increase in the first minute that is attributed to peripheral chemoreceptors, followed by a centrally-mediated secondary depression over several minutes to a new steady-state phase II level. Our data complement emerging evidence of a central component to the excitation where glia act as hypoxia sensors and release ATP, exciting the respiratory network and offsetting the secondary respiratory depression (Angelova *et al.* 2015; Gourine & Funk, 2017). We advance the current mechanistic understanding by showing that the actions of ATP in the HVR are mediated in the preBötC through activation of P2Y₁ receptors that increase inspiratory frequency *in vitro* via thapsigargin-sensitive increases in $[Ca^{2+}]_i$ occurring in both inspiratory neurons and astroglia. Given the significant developmental changes that occur in both neuronal, and presumably glial (Zhou *et al.* 2006), components of the respiratory network, important future objectives will include assessing whether the mechanisms of P2Y₁ receptor-mediated signalling defined here in neonates *in vitro* apply in adults during hypoxia and whether changes in glial signalling contribute to the greater hypoxic respiratory depression in prematurity. The fact that the P2Y₁ receptor-mediated excitation of the preBötC network, defined first in rhythmic slices (Funk *et al.* 1997; Lorier *et al.* 2004, 2007, 2008; Huxtable *et al.* 2009; Zwicker *et al.* 2011), is a major contributor to the excitatory actions of ATP released *in vivo* in hypoxia suggests that the combined *in vitro*–*in vivo* approach employed here will continue to be most insightful (Gourine & Funk, 2017).

The role of glia and ATP in phase I and phase II of the hypoxic ventilatory response

Evidence for gliotransmission in the intact CNS is sparse, reflecting the difficulty of selectively manipulating glial function. The contribution of gliotransmission to the HVR was first demonstrated by the reduction of the HVR in freely-moving rats following blockade of glial exocytosis through bilateral expression of TeLC in preBötC/VRC astrocytes (Angelova *et al.* 2015). In the present study, in paralysed, mechanically ventilated rats, blockade of vesicular transmitter release in glia using TeLC suggests that gliotransmission contributes to both phases of the HVR.

Unilateral microinjection of MRS 2279 into the preBötC, in contrast, did not affect the phase I increase, indicating that P2Y₁ receptors in the preBötC do not contribute. Two protocol differences might account for this discrepancy. First, because TeLC blocks all vesicular release mechanisms but MRS 2279 selectively antagonizes P2Y₁ receptors, the reduction of ventilation in phase I in conditions of TeLC expression in preBötC astrocytes may indicate a contribution of a non-P2Y₁ receptor-mediated component. Astrocytes release multiple transmitters, including glutamate and D-serine, that could stimulate ventilation. ATP evokes glutamate release from cultured preBötC glia (Huxtable *et al.* 2010), although stimulation of glia in rhythmic slices with ATP does not cause glutamatergic excitation of inspiratory neurons (Fig. 13).

Second, the region of the brainstem affected was different between TeLC and MRS 2279 protocols. Viral injections were bilateral and centered in the preBötC, although expression extended > 500 μ m rostrally and caudally from the centre of the injection site in preBötC. The MRS 2279 injections were unilateral and, if MRS 2279 and DLH have similar diffusion profiles, probably extended less than 200 μ m. Given that the bulk of evidence supports that the phase I response is mediated by carotid body chemoreceptors (Bureau *et al.* 1985; Fung *et al.* 1996; Prabhakar, 2000), the physiological significance of the inhibition of the phase I response mediated by expression of TeLC in astrocytes must be interpreted cautiously until the underlying mechanism is established.

Our conclusion that gliotransmission contributes to the HVR depends on the selectivity of the bidirectional sGFAP-based vector system to interfere with exocytosis only in astrocytes. Glial specificity of this vector system (Liu *et al.* 2008; Gourine *et al.* 2010; Tang *et al.* 2014) and efficacy of TeLC in blocking exocytosis have been demonstrated (Angelova *et al.* 2015). Our analysis of transfected brain sections further suggests that TeLC expression is specific to astrocytes when under the control of the sGFAP promoter; no cells were detected that expressed eGFP and displayed NeuN immunoreactivity.

ATP acts via P2Y₁ receptors to increase ventilation *in vivo*

P2 receptors comprise seven ionotropic P2X (North, 2002) and eight metabotropic P2Y (Abbracchio *et al.* 2003) subtypes. P2Y₁ receptor immunolabelling is prevalent throughout the VLM (Fong *et al.* 2002) and overlaps with intense NK1 receptor expression, an established marker of the preBötC. Indeed, P2Y₁ receptors underlie the excitatory actions of ATP in the preBötC *in vitro* (Lorier *et al.* 2007). In the present study, we translate these *in vitro* findings and reveal, using unilateral injections of MRS 2279, that endogenous activation of preBötC P2Y₁ receptors *in vivo* increases ventilation and attenuates the secondary hypoxic respiratory depression. The fact that antagonists were only applied unilaterally means that our measurements may underestimate the magnitude of the P2Y₁ receptor-mediated increases in ventilation during hypoxia. Whether P2Y₁ receptors are the only P2 receptor subtype involved in the HVR is uncertain because a variety of P2 receptors are expressed in the VRC (Thomas *et al.* 2001; Fong *et al.* 2002; Gourine *et al.* 2003; Lorier *et al.* 2004, 2007). Nonetheless, our data illustrate a significant role for P2Y₁R in the ATP-induced increase in ventilation in the preBötC during hypoxia.

Adenosine inhibition of the preBötC network does not contribute to the hypoxic respiratory depression in adult rat

Experiments were not designed to identify the mechanisms underlying the hypoxic respiratory depression, although our data provide some insight. First, the P2Y₁ receptor-mediated attenuation indicates that the secondary depression is not shaped by a single inhibitory mechanism. Second, adenosine inhibition of the preBötC network does not contribute to the depression in adult rats. The enhanced hypoxic respiratory depression observed in adult rats expressing the ectonucleotidase TMPAP in the preBötC and VRC (Angelova *et al.* 2015) is a result of degradation of excitatory ATP rather than accumulation of adenosine. Also, hypoxia-induced adenosine release has been detected in the nucleus tractus solitarius of adult rats, but not in the VLM (Gourine *et al.* 2002).

Developmentally, adenosine plays a more important role. An A1 receptor inhibitory mechanism is implicated in the secondary hypoxic depression in a host of premature/newborn mammals including pigs, sheep (Moss, 2000), rats and mice (Funk *et al.* 2008; Huxtable *et al.* 2009; Zwicker *et al.* 2011). Developmental analyses are required in multiple species to assess whether A1 inhibitory mechanisms disappear postnatally, as occurs in P2–3 rats (Herlenius *et al.* 1997; Huxtable *et al.* 2009). Medullary and suprapontine A2a receptor-mediated excitation of GABAergic inhibitory neurons may also contribute to the

depression in piglets and fetal sheep (Koos & Maeda, 2001; Koos *et al.* 2001; Wilson *et al.* 2004), although these actions do not appear to be through A2a receptor mechanisms in the preBötC because inhibition of rhythm by adenosine within the preBötC (in rats and mice) is completely blocked by the A1 receptor antagonist DPCPX (Huxtable *et al.* 2009; Zwicker *et al.* 2011).

Signalling pathways of the P2Y₁ receptor-mediated excitation; neurons vs. glia

The only identified source of extracellular ATP during hypoxia is from astrocytes (Angelova *et al.* 2015). Thus, our working hypothesis is that, during hypoxia, astrocyte-derived ATP increases inspiratory frequency not only through excitation of preBötC inspiratory neurons, but also through autocrine/paracrine excitation of astrocytes causing further gliotransmitter release (Fig. 1 iii, vi). Consistent with this hypothesis, both preBötC inspiratory neurons (in slices) (Fig. 11) and preBötC glia (in slices and culture) (Fig. 12) (Huxtable *et al.* 2010) respond to ATP via a P2Y₁ receptor signalling pathway that involves a thapsigargin-sensitive increase in $[Ca^{2+}]_i$ and a neuronal inward current (Lorier *et al.* 2008). The ion channels underlying this inward current have yet to be identified, although candidates have been proposed (Rajani *et al.* 2015).

ATP-induced excitation of neurons is clearly involved in preBötC excitation. However, a role for autocrine/paracrine excitation of astrocytes by ATP remains to be established. Autocrine/paracrine excitation was first implicated with the observations that glial toxins attenuate the frequency increase evoked by ATP in the preBötC *in vitro* and that cultured preBötC astrocytes release glutamate in response to ATP (Huxtable *et al.* 2010). By contrast, imaging of cultured brainstem astrocytes suggests that ATP does not signal via paracrine/autocrine mechanisms; low pH and hypoxia-evoked fusion of putative ATP-containing vesicles was unaffected by ATP degrading enzymes or P2Y₁ receptor antagonists (Kasymov *et al.* 2013; Angelova *et al.* 2015). The sparse nature of these astrocyte cultures could have compromised the detection of autocrine/paracrine signalling. However, our whole-cell data showing that ATP does not evoke glutamatergic excitation of inspiratory neurons suggest that preBötC astrocytes *in situ* do not respond to ATP by releasing a transmitter, and that autocrine/paracrine ATP signalling may not contribute to the HVR.

$[Ca^{2+}]_i$ increases contribute to P2Y₁ receptor-mediated inspiratory frequency increase

Analysis of recombinant receptors suggests that P2Y₁ receptors predominantly signal through the G_{αq/11} pathway, which involves activation of PLC, release

of Ca²⁺ from intracellular stores and DAG-mediated activation of protein kinase C (Simon *et al.* 1995; von Kugelgen & Wetter, 2000; Sak & Illes, 2005). In the present study, we show that an increase in [Ca²⁺]_i contributes to the P2Y₁-mediated frequency increase *in vitro*, which implicates a Ca²⁺-dependent, second messenger pathway that is dependent on [Ca²⁺]_i. The ATP/MRS 2365-mediated frequency increase, however, was not completely blocked by EGTA-AM or thapsigargin (Fig. 10). Thus, either the blockade of [Ca²⁺]_i changes was incomplete or Ca²⁺-insensitive pathways may contribute. P2Y₁ receptors can also signal through Gα_i and alter ion channel activity through the membrane-delimited βγ subunit without changing [Ca²⁺]_i (Brown *et al.* 2000; Filippov *et al.* 2000; Aoki *et al.* 2004). To fully clarify these mechanisms, a deeper exploration of signalling pathways and downstream candidate ion channels underlying the P2Y₁-evoked excitation of the preBötC is required (Rajani *et al.* 2015).

Significance

Understanding the multitude of factors that determine the dynamics of the HVR is key in the development of strategies to counteract the hypoxia-induced depression of breathing. We have identified an endogenous P2Y₁ receptor mechanism that attenuates this depression in adults and is active in embryonic stages through to adulthood in mammals. Degradation of ATP in the preBötC will contribute to the depression not only by removing the excitatory actions of ATP, but also by producing adenosine, which is inhibitory in the perinatal period and has variable effects into adulthood. Strategies aiming to minimize the hypoxic depression of ventilation should aim to enhance P2Y₁ receptor-mediated signalling, inhibit ATP degradation and enhance the removal of adenosine from the extracellular space of the brainstem.

References

- Abbracchio MP, Boeynaems J-M, Barnard EA, Boyer JL, Kennedy C, Miras-Portugal MT, King BF, Gachet C, Jacobson KA, Weisman GA & Burnstock G (2003). Characterization of the UDP-glucose receptor (re-named here the P2Y₁₄ receptor) adds diversity to the P2Y receptor family. *Trends Pharmacol Sci* **24**, 52–55.
- Angelova PR, Kasymov V, Christie I, Sheikhabaehi S, Turovsky E, Marina N, Korsak A, Zwicker J, Teschemacher AG, Ackland GL, Funk GD, Kasparov S, Abramov AY & Gourine AV (2015). Functional oxygen sensitivity of astrocytes. *J Neurosci* **35**, 10460–10473.
- Aoki Y, Yamada E, Endoh T & Suzuki T (2004). Multiple actions of extracellular ATP and adenosine on calcium currents mediated by various purinoceptors in neurons of nucleus tractus solitarius. *Neurosci Res* **50**, 245–255.
- Boutin RC, Alsaifi Z & Pagliardini S (2017). Cholinergic modulation of the parafacial respiratory group. *J Physiol* **595**, 1377–1392.
- Brown DA, Filippov AK & Barnard EA (2000). Inhibition of potassium and calcium currents in neurones by molecularly-defined P2Y receptors. *J Auton Nerv Syst* **81**, 31–36.
- Bureau MA, Lamarche J, Foulon P & Dalle D (1985). The ventilatory response to hypoxia in the newborn lamb after carotid body denervation. *Respir Physiol* **60**, 109–119.
- Filippov AK, Brown DA & Barnard EA (2000). The P2Y₁ receptor closes the N-type Ca²⁺ channel in neurones, with both adenosine triphosphates and diphosphates as potent agonists. *Br J Pharmacol* **129**, 1063–1066.
- Fong AY, Krstew EV, Barden J & Lawrence AJ (2002). Immunoreactive localisation of P2Y₁ receptors within the rat and human nodose ganglia and rat brainstem: comparison with [alpha-³³P]deoxyadenosine 5'-triphosphate autoradiography. *Neuroscience* **113**, 809–823.
- Fung ML, Wang W, Darnall RA & St John WM (1996). Characterization of ventilatory responses to hypoxia in neonatal rats. *Respir Physiol* **103**, 57–66.
- Funk G, Huxtable A & Lorier A (2008). ATP in central respiratory control: a three-part signaling system. *Respir Physiol Neurobiol* **164**, 131–142.
- Funk GD (2013). Neuromodulation: purinergic signaling in respiratory control. *Compr Physiol* **3**, 331–363.
- Funk GD & Greer JJ (2013). The rhythmic, transverse medullary slice preparation in respiratory neurobiology: Contributions and caveats. *Respiratory Physiology & Neurobiology* **186**, 236–253.
- Funk GD, Kanjhan R, Walsh C, Lipski J, Comer AM, Parkis MA & Housley GD (1997). P2 receptor excitation of rodent hypoglossal motoneuron activity in vitro and in vivo: a molecular physiological analysis. *J Neurosci* **17**, 6325–6337.
- Gourine AV, Atkinson L, Deuchars J & Spyer KM (2003). Purinergic signalling in the medullary mechanisms of respiratory control in the rat: respiratory neurones express the P2X₂ receptor subunit. *J Physiol* **552**, 197–211.
- Gourine AV & Funk GD (2017). On the existence of a central respiratory oxygen sensor. *J Appl Physiol* (1985), jap 00194 02017.
- Gourine AV, Kasymov V, Marina N, Tang F, Figueiredo MF, Lane S, Teschemacher AG, Spyer KM, Deisseroth K & Kasparov S (2010). Astrocytes control breathing through pH-dependent release of ATP. *Science* **329**, 571–575.
- Gourine AV, Llaudet E, Dale N & Spyer KM (2005). Release of ATP in the ventral medulla during hypoxia in rats: role in hypoxic ventilatory response. *J Neurosci* **25**, 1211–1218.
- Gourine AV, Llaudet E, Thomas T, Dale N & Spyer KM (2002). Adenosine release in nucleus tractus solitarius does not appear to mediate hypoxia-induced respiratory depression in rats. *J Physiol* **544**, 161–170.
- Gray PA, Janczewski WA, Mellen N, McCrimmon DR & Feldman JL (2001). Normal breathing requires preBötzing complex neurokinin-1 receptor-expressing neurons. *Nat Neurosci* **4**, 927–930.

- Gray PA, Rekling JC, Bocchiaro CM & Feldman JL (1999). Modulation of respiratory frequency by peptidergic input to rhythmogenic neurons in the preBötzinger complex. *Science* **286**, 1566–1568.
- Guyenet PG, Sevigny CP, Weston MC & Stornetta RL (2002). Neurokinin-1 receptor-expressing cells of the ventral respiratory group are functionally heterogeneous and predominantly glutamatergic. *J Neurosci* **22**, 3806–3816.
- Guyenet PG & Wang H (2001). Pre-Bötzinger neurons with preinspiratory discharges ‘in vivo’ express NK1 receptors in the rat. *J Neurophysiol* **86**, 438–446.
- Herlenius E, Lagercrantz H & Yamamoto Y (1997). Adenosine modulates inspiratory neurons and the respiratory pattern in the brainstem of neonatal rats. *Pediatr Res* **42**, 46–53.
- Horner RL (2012). Neural control of the upper airway: integrative physiological mechanisms and relevance for sleep disordered breathing. *Compr Physiol* **2**, 479–535.
- Huxtable AG, Zwicker JD, Alvares TS, Ruangkittisakul A, Fang X, Hahn LB, Posse de Chaves E, Baker GB, Ballanyi K & Funk GD (2010). Glia contribute to the purinergic modulation of inspiratory rhythm-generating networks. *J Neurosci* **30**, 3947–3958.
- Huxtable AG, Zwicker JD, Poon BY, Pagliardini S, Vrouwe SQ, Greer JJ & Funk GD (2009). Tripartite purinergic modulation of central respiratory networks during perinatal development: the influence of ATP, ectonucleotidases, and ATP metabolites. *J Neurosci* **29**, 14713–14725.
- Kasymov V, Larina O, Castaldo C, Marina N, Patrushev M, Kasparov S & Gourine AV (2013). Differential sensitivity of brainstem versus cortical astrocytes to changes in pH reveals functional regional specialization of astroglia. *J Neurosci* **33**, 435–441.
- Koos BJ & Maeda T (2001). Adenosine A(2A) receptors mediate cardiovascular responses to hypoxia in fetal sheep. *Am J Physiol Heart Circ Physiol* **280**, H83–H89.
- Koos BJ, Maeda T & Jan C (2001). Adenosine A(1) and A(2A) receptors modulate sleep state and breathing in fetal sheep. *J Appl Physiol* (1985) **91**, 343–350.
- Liu B, Paton JF & Kasparov S (2008). Viral vectors based on bidirectional cell-specific mammalian promoters and transcriptional amplification strategy for use in vitro and in vivo. *BMC Biotechnol* **8**, 49.
- Lorier AR, Huxtable AG, Robinson DM, Lipski J, Housley GD & Funk GD (2007). P2Y1 receptor modulation of the pre-Botzinger complex inspiratory rhythm generating network in vitro. *J Neurosci* **27**, 993–1005.
- Lorier AR, Lipski J, Housley GD, Greer JJ & Funk GD (2008). ATP sensitivity of preBötzinger complex neurones in neonatal rat in vitro: mechanism underlying a P2 receptor-mediated increase in inspiratory frequency. *J Physiol* **586**, 1429–1446.
- Lorier AR, Peebles K, Brosenitsch T, Robinson DM, Housley GD & Funk GD (2004). P2 receptors modulate respiratory rhythm but do not contribute to central CO₂ sensitivity in vitro. *Respir Physiol Neurobiol* **142**, 27–42.
- Monnier A, Alheid GF & McCrimmon DR (2003). Defining ventral medullary respiratory compartments with a glutamate receptor agonist in the rat. *J Physiol* **548**, 859–874.
- Moss IR (2000). Respiratory responses to single and episodic hypoxia during development: mechanisms of adaptation. *Respir Physiol* **121**, 185–197.
- North RA (2002). Molecular physiology of P2X receptors. *Physiol Rev* **82**, 1013–1067.
- Paxinos G & Watson C (2007). *The Rat Brain in Stereotaxic Coordinates*. Academic Press, Boston, MA.
- Prabhakar NR (2000). Oxygen sensing by the carotid body chemoreceptors. *J Appl Physiol* **88**, 2287–2295.
- Rajani V, Zhang Y, Revill AL & Funk GD (2015). The role of P2Y receptor signaling in central respiratory control. *Respir Physiol Neurobiol* **226**, 3–10.
- Ramirez JM, Quellmalz UJ & Richter DW (1996). Postnatal changes in the mammalian respiratory network as revealed by the transverse brainstem slice of mice. *J Physiol* **491**, 799–812.
- Ruangkittisakul A, Panaitescu B, Secchia L, Bobocea N, Kantor C, Kuribayashi J, Iizuka M & Ballanyi K (2012). Anatomically ‘calibrated’ isolated respiratory networks from newborn rodents. In *Isolated Central Nervous System Circuits*, ed. Ballanyi K, pp. 61–124. Humana Press, Totowa, NJ.
- Ruangkittisakul A, Schwarzacher SW, Secchia L, Ma Y, Bobocea N, Poon BY, Funk GD & Ballanyi K (2008). Generation of eupnea and sighs by a spatiochemically organized inspiratory network. *J Neurosci* **28**, 2447–2458.
- Ruangkittisakul A, Schwarzacher SW, Secchia L, Poon BY, Ma Y, Funk GD & Ballanyi K (2006). High sensitivity to neuromodulator-activated signaling pathways at physiological [K⁺] of confocally imaged respiratory center neurons in on-line-calibrated newborn rat brainstem slices. *J Neurosci* **26**, 11870–11880.
- Sak K & Illes P (2005). Neuronal and glial cell lines as model systems for studying P2Y receptor pharmacology. *Neurochem Int* **47**, 401–412.
- Simon J, Webb TE, King BF, Burnstock G & Barnard EA (1995). Characterisation of a recombinant P2Y purinoceptor. *Eur J Pharmacol* **291**, 281–289.
- Smith J, Ellenberger H, Ballanyi K & Richter D (1991). Pre-Botzinger complex: a brainstem region that may generate respiratory rhythm in mammals. *Science* **254**, 726–729.
- So EL (2008). What is known about the mechanisms underlying SUDEP? *Epilepsia* **49** (Suppl 9), 93–98.
- Spitzer M, Wildenhain J, Rappsilber J & Tyers M (2014). BoxPlotR: a web tool for generation of box plots. *Nat Methods* **11**, 121–122.
- Tang F, Lane S, Korsak A, Paton JFR, Gourine AV, Kasparov S & Teschemacher AG (2014). Lactate-mediated glia-neuronal signalling in the mammalian brain. *Nat Commun* **5**, 3284.
- Teppema LJ & Dahan A (2010). The ventilatory response to hypoxia in mammals: mechanisms, measurement, and analysis. *Physiol Rev* **90**, 675–754.
- Thomas T, Ralevic V, Bardini M, Burnstock G & Spyer KM (2001). Evidence for the involvement of purinergic signalling in the control of respiration. *Neuroscience* **107**, 481–490.
- von Kugelgen I & Wetter A (2000). Molecular pharmacology of P2Y-receptors. *Naunyn Schmiedeberg Arch Pharmacol* **362**, 310–323.

- Wilson CG, Martin RJ, Jaber M, Abu-Shaweesh J, Jafri A, Haxhiu MA & Zaidi S (2004). Adenosine A2A receptors interact with GABAergic pathways to modulate respiration in neonatal piglets. *Respir Physiol Neurobiol* **141**, 201–211.
- Zhou M, Schools GP & Kimelberg HK (2006). Development of GLAST(+) astrocytes and NG2(+) glia in rat hippocampus CA1: mature astrocytes are electrophysiologically passive. *J Neurophysiol* **95**, 134–143.
- Zwicker JD, Rajani V, Hahn LB & Funk GD (2011). Purinergic modulation of preBötzinger complex inspiratory rhythm in rodents: the interaction between ATP and adenosine. *J Physiol* **589**, 4583–4600.

Additional information

Competing interests

The authors declare that they have no competing interests.

Author contribution

Experiments were performed in the laboratories of GDF (University of Alberta, Canada), AVG (University College London, UK), SK (University of Bristol, UK), KB (University of Alberta, Canada) and SP (University of Alberta, Canada). VR, YZ, VJ, JDZ, SP, CTD, KB, SK, AVG and GDF all contributed to the conception and design of the work. All authors contributed to acquisition, analysis or interpretation of data for the work,

as well as drafting the final work or revising it critically for important intellectual content. All authors approved the final version of the manuscript submitted for publication and agree to be accountable for all aspects of the work. All persons designated as authors qualify for authorship, and all those who qualify for authorship are listed.

Funding

This work was supported by the Canadian Institutes for Health Research (CIHR, 53085 to GDF; GSD-121789 to VR), National Sciences and Engineering Research Council (NSERC, 402532 to GDF; 435843 to SP), Alberta Innovates Health Solutions (AIHS), University Hospital Foundation (Hochausen Fund) (KB), Women and Children's Health Research Foundation, Canadian Foundation for Innovation (CFI), Alberta Science and Research Authority (ASRA), the Wellcome Trust (Grants 095064 and 200893 to AVG), BBSRC (MR/L020661/1 and BB/L019396/1 to SK) and the Intramural Research Program of the NIH, NINDS (SSB). SSB is a NIH-UCL GPP fellow.

Acknowledgements

We thank Dr Elena Posse de Chaves (University of Alberta, Canada) for her assistance with glial culture experiments. We also thank Tucauê S. Alvares for his technical assistance with all experiments performed at the University of Alberta.